Impurity-generated non-Abelions

G. Simion, A. Kazakov, L. P. Rokhinson, T. Wojtowicz, and Y. B. Lyanda-Geller

Phys. Rev. B **97**, 245107 — Published 7 June 2018

DOI: 10.1103/PhysRevB.97.245107

Impurity-generated non-Abelions

G. Simion,[1] A. Kazakov,[1] L. P. Rokhinson,[1,2,3]

T. Wojtowicz,[4,5] and Y. B. Lyanda-Geller[1,2,*]

[1]*Department of Physics and Astronomy,*

Purdue University, West Lafayette, IN 47907 USA

[2]*Birck Nanotechnology Center, Purdue University, West Lafayette, IN 47907 USA*

[3]*Department of Electrical and Computer Engineering,*

Purdue University, West Lafayette, IN 47907 USA

[4]*International Research Centre MagTop,*

Aleja Lotnikow 32/46, PL-02668 Warsaw, Poland

[5]*Institute of Physics, Polish Academy of Sciences,*

Al. Lotnikow 32/46, 02-668 Warsaw, Poland

(Dated: July, 12 2017)

Abstract

Two classes of topological superconductors and Majorana modes in condensed matter systems are known to date: one, in which disorder induced by impurities strongly suppresses topological superconducting gap and is detrimental to Majorana modes, and the other, where Majorana fermions are protected by disorder-robust topological superconductor gap. Observation and control of Majorana fermions and other non-Abelions often requires a symmetry of an underlying system leading to a gap in a single-particle or quasiparticle spectra. In semiconductor structures impurities that provide charge carriers introduce states into the gap and enable conductance and proximity-induced superconductivity via the in-gap states. Thus, a third class of topological superconductivity and Majorana modes emerges, in which topological superconductivity and Majorana fermions appear exclusively when impurities generate in-gap states. We show that impurity-enabled topological superconductivity is realized in a quantum Hall ferromagnet, when helical domain wall is coupled to an s-wave superconductor. As an example of emergence of topological superconductivity in quantum Hall ferromagnets, we consider integer quantum Hall effect in Mn doped CdTe quantum wells. Recent experiments on transport through the quantum Hall ferromagnet domain wall in this system indicated a vital role of impurities in the conductance, but left an unresolved the question whether impurities preclude generation of Majorana fermions and other non-Abelions in such systems in general. Here, solving a general quantum mechanical problem of impurity bound states in a system of spin-orbit coupled Landau levels, we demonstrate that impurity-induced Majorana modes emerge at boundaries between topological and conventional superconducting states generated in a domain wall due to proximity to an s-superconductor. We consider both short range disorder and smooth random potential. The phase diagram of the system is defined by characteristic disorder, gate voltage induced angular momentum splitting of impurity levels and by proximity superconducting gap. The phase diagram exhibits two ranges of gate voltage with conventional superconducting order separated by a gate voltage range with topological superconductivity. We show that electrostatic control of domain walls in an integer quantum Hall ferromagnet allows manipulation of Majorana fermions. Ferromagnetic transitions in the fractional quantum Hall regime may lead to the formation and electrostatic control of higher order non-Abelian excitations.

* yuli@purdue.edu

I. INTRODUCTION

Non-abelions in solid state systems, such as Majorana fermions, parafermions or Fibonacci anyons, result in topologically degenerate ground state characterized by non-Abelian statistics and provide paths to topological fault-tolerant quantum computing [1, 2]. Exotic states with non-Abelian excitations are predicted to emerge in correlated states in the fractional quantum Hall regime in two-dimensional electron, bilayer and hole gases [3–9], in p-wave ^{3}He [10], and in hybrid superconductor/topological insulator [11, 12] and superconductor/semiconductor [13–16] systems. Topological superconductors can be divided into two broad classes: one, in which disorder induced by impurities strongly suppresses topological superconducting gap and can be detrimental to non-Abelions [17–23], and the other, in which non-Abelian excitations are protected by an impurity-robust topological superconductor gap [24–32]. In semiconductor wires impurity scattering can change the range of parameters characterizing topological superconductivity without changes in mechanisms of superconducting proximity effect or conductance through the system [33]. In this work, we present a third class of topological superconductivity and Majorana fermions, which appear exclusively when impurities generate states in gapped energy spectrum, enabling conductance through the system and a superconducting proximity effect via the in-gap states.

Observation and control of Majorana fermions and other non-Abelions often require a symmetry of an underlying system leading to a gap in a single-particle or a quasiparticle spectra. An example is a quantum Hall system proximity-coupled to a superconductor, where Majorana fermions [34], parafermions [35], and Fibonacci fermions [36] are predicted to be formed in the presence of interacting counter-propagating edge channels. Realizations of non-Abelions in quantum Hall systems coupled to a superconductor have a very important feature: a superconductor in this case couples effectively to a single electron channel (two counterpropagating channels). This precludes many complications that may emerge, e.g, in Majorana quantum wire settings, when several electron channels can be occupied in wires in proximity of a superconductor. Emergence of higher order non-Abelian excitations, such as parafermions and Fibonacci anyons in quantum Hall based systems is the other reason why such system have potential advantage.

Emerging experiments in quantum Hall systems with counterpropagating edge channels indicate strong level repulsion and opening of a large exchange gap for interacting edge

channels with the same orbital quantum numbers[37]. A promising alternative is a quantum Hall ferromagnetic transition, where domain walls at a filling factor $\nu = 1$ have helical magnetic order[38]. However, when helical domain walls are formed from almost orthogonal states with different orbital quantum numbers and opposite spins in integer and fractional QHE regimes, spin-orbit interactions open small spectral gaps in bulk Landau level spectrum [37] and in the spectra of electrostatically induced edge states [39]. These gaps suppress electron transport at low temperatures [37, 40], but in short helical domain walls transport can be carried by the in-gap states [39]. This mechanism is important experimentally, because it becomes possible to distinguish conductance through a single domain wall from conductance through the bulk of the 2D gas.

Here we demonstrate that impurity-induced in-gap states in electrostatically defined helical domain walls can lead to topological superconductivity when coupled to an s-wave superconductor. We solve a general quantum mechanical problem of short-range impurity states in the presence of Landau quantization and spin-orbit interactions, and derive impurity states in the electrostatically induced domain wall. We then map the system of these states on the analog of a generalized Kitaev chain [24, 41], and calculate the phase diagram for the existence of topological superconductivity and Majorana fermions. Because the origin of the system is helical edge states, which yield the spectrum of impurity system with wide range of energy separations of states with distinct angular momentum, the generalized Kitaev chain in our case has different symmetry properties and a different phase diagram compared to regular Kitaev chain or a chain of quantum dots [24]. We extend our consideration to impurities resulting in a smooth random potential, and demonstrate that topolological superconductivity and Majorana fermions also emerge in that case. Finally, we demonstrate that with a local electrostatic control of the QHFm transition it is possible to induce, move, exchange, fuse and braid Majorana modes.

We consider a specific case of a 2D electron gas formed in asymmetrically Mn-doped CdTe quantum wells, where local electrostatic control of a quantum Hall ferromagnetic transition and a single helical domain wall manipulation have been recently reported [39]. However, these experiments indicated the vital role of impurities in conductance through electrostatically controlled individual domain wall in this system, and raised the question whether this intrinsically precludes generation of Majorana fermions and other non-Abelions in quantum Hall ferromagnets or if the non-Abelions are still feasible. We resolve this

problem affirmatively, showing that impurities are crucial for generating non-Abelions. Our conclusions should be applicable to any system where quantum Hall ferromagnetic transition can be locally controlled, such as, e.g., a 2D hole gas in Ge[42]. Quantum Hall ferromagnetic transitions in the integer and fractional QHE regimes have been observed in 2D gases in many semiconductors, including GaAs [40, 43], AlAs [44], InSb [45], CdMnTe [46, 47], Si [48] and graphene [49], and their electrostatic control has been shown [37, 50, 51].

II. MAJORANA MODES IN A HELICAL DOMAIN WALL

In Mn-doped CdTe quantum wells external magnetic field $\mathbf{B}$ aligns spins of Mn^{2+} ions and generates an additional exchange contribution to the electron spin splitting due to interactions between conduction electrons and d-shell electrons localized on Mn [52]. This s-d exchange splitting has a sign opposite to the bare Zeeman splitting for electrons in the conduction band, leading to multiple level crossings at high magnetic fields [46]. The ferromagnetic transition of interest occurs at a crossing of states with opposite polarizations belonging to the first two Landau levels $(n = 0, \uparrow)$ and $(n = 1, \downarrow)$ at a filling factor $\nu = 2$. In an asymmetrically Mn-doped quantum wells the strength of the s-d exchange can be electrostatically controlled [37] and it is possible to form an unpolarized and a fully polarized states under different gates,as shown schematically in Fig. 1.

In order to describe a helical domain wall formed between the gates we consider the edge-like states in a quantum Hall system induced by an electrostatic potential $V(z, x)$ uniform along the y-direction and varying between V_1 and V_2 in the x-direction between the two gates, Fig. 1. We call these states edge-like in order to distinguish them from the conventional edge states flowing at the physical boundary of the 2D sample. In much the same way as Landau spectrum is prominent when the cyclotron energy greatly exceeds the Landau level broadening, such edge-like states and a domain wall are formed as soon as electrostatic potential introduces energy difference between the two areas underneath the gates V_1 and V_2 that sufficiently exceeds the level broadening. The effective 2D electron Hamiltonian is given by

$$H = -\frac{1}{2m^*}\left(-i\hbar\nabla - \frac{e\mathbf{A}}{c}\right)^2 + e\mathcal{E}_x x + \frac{1}{2}\sigma_z(\frac{1}{2}g^*\mu_B B + J_0 + J_1 x)\ , \qquad (1)$$

where $\mathbf{A}$ is a vector potential of a magnetic field $\mathbf{B} = \boldsymbol{\nabla} \times \mathbf{A}$, which is directed along

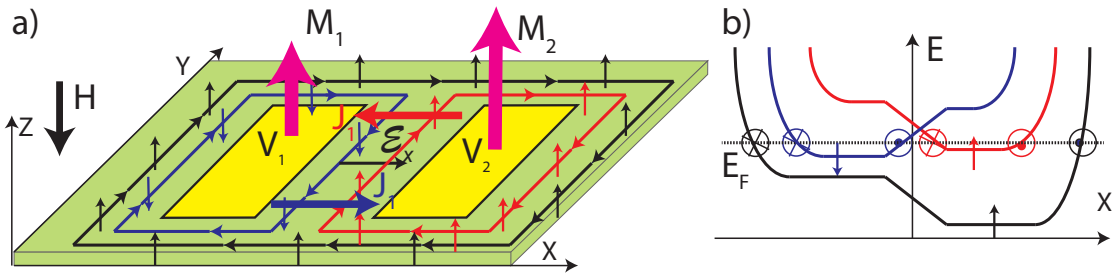

FIG. 1. a) Electrostatic gates V_1 and V_2 control magnetization $\mathbf{M_1}$ and $\mathbf{M_2}$ caused by the electron exchange interactions with Mn impurities. A spatial gradient of magnetization J_1 and a potential gradient $\mathcal{E}_x$ result in the formation of edge-like states between the gates (red and blue). Vertical arrows along edge states show spin polarization of electrons, which is opposite for edge-like states as a result of quantum Hall ferromagnetic transition. Between the gates edge-like states are hybridized and form a helical domain wall. b) Energy profile of electron states in the absence of spin-orbit interactions. Due to different polarization of red and blue states, the electron system at $\nu = 2$, which also include electrons in the ground Landau level (black), are unpolarized on the left and polarized on the right.

negative z, $B = |B_z|$, m^*, e and g^* are electron effective mass, charge, and g-factor, $\vec{\sigma}$ is the Pauli matrix vector, σ_z is its z-component, μ_B is the Bohr magneton, and $\mathcal{E}_x = -\nabla_x \int \phi^*(z)V(z,x)\phi(z)dz$ is an electric field in x-direction caused by the gradient of the gate-induced potential $V(z,x)$, $\phi(z)$ is the $z-$envelope of the wavefunction. In the mean field approximation, s-d exchange interactions are represented by a uniform part J_0 and a gate-induced variation of the s-d exchange $J_1 x$ [53]. J_1 constitutes a spin-dependent electric field in x-direction. As was demonstrated in [37], using a combination of front and back gates and for a non-uniform doping of the quantum well by Mn^{2+} ions along the growth direction z, it is possible to achieve almost uniform 2D electron density but induce significant $J_1 \gg e\mathcal{E}_x$, [53]. While considering nonzero $\mathcal{E}_x$ will not change our essential results, we will keep only J_1 effective spin electric field and take $\mathcal{E}_x = 0$.

In this model, the electron eigenvalues and wavefunctions are

$$E_{n,s,k_y} = \hbar\omega_c\left(n + \frac{1}{2}\right) + \hbar k_y v_s - \frac{m^* v_s^2}{2} - s(\frac{1}{2}g^*\mu_B B + J_0) \tag{2}$$

$$\psi_{n,s,k_y} = u_n\left(x - k_y\ell^2 + \frac{v_s}{\omega_c}\right)e^{ik_y y}\chi_s \ , \tag{3}$$

where $\omega_c = eB/(m^*c)$ is the cyclotron frequency, $\ell = (eB/\hbar c)^{-1/2}$ is the magnetic length, k_y is the y-component of the wavevector $\vec{k}$, u_n are the Landau wavefunctions, $s = \pm 1$ is for spins up and down, $\chi_1 = \chi_\uparrow = (1,0)^T$ and $\chi_{-1} = \chi_\downarrow = (0,1)^T$. The spin-dependent drift velocity $v_s = s \cdot v$, where $v = cJ_1/2eB$. At $\nu = 2$ the edge-like states, Eq. 2, are localized near the spectral crossing of $(n = 0, \downarrow)$ and $(n = 1, \uparrow)$ states and can propagate between the two gated regions with opposite velocities.

A non-magnetic disorder cannot cause scattering between two edge-like states (3) due to their opposite spins. However, two edges with opposite velocities originating from neighboring Landau levels are coupled by spin-orbit interactions, similar to the coupling of edges in a 2D topological insulator introduced by an in-plane Zeeman field. The specific mechanism of such coupling between zeroth Landau level spin down and first Landau level spin up states is Rashba (but not the Dresselhaus) spin-orbit interactions, described by a 2D Hamiltonian $H_R = \gamma_R \mathcal{E}_z (\vec{\sigma} \times \vec{k})_z$. Here $\mathcal{E}_z$ is the component of the electric field perpendicular to the 2D plane, and γ_R is the Rashba coefficient. The resulting spin-orbit coupling $h_R = \int \psi^*_{0,downarrow,k_y} H_R \psi_{1,\uparrow,k_y} dxdy$ is given by

$$h_R = \sqrt{2} \frac{\gamma_R \mathcal{E}_z}{\ell} e^{-\frac{m^2\ell^2}{\hbar^2}v^2} \left[1 - \frac{m^2\ell^2}{\hbar^2} v^2\right] \ . \tag{4}$$

In the presence of this spin-orbit coupling, the effective single-particle Hamiltonian in the basis of the $(n = 0, \downarrow)$ and $(n = 1, \uparrow)$ states (2) near their spectral crossing is given by

$$H_e = hk_y v\sigma_z + h_R \sigma_x \ . \tag{5}$$

Thus, this single-particle system, which serves as a setting for the proximity-induced topological superconductivity, is rather unusual: in contrast to the nanowires and topological insulators, where spin-orbit interactions result in the level crossing and the Zeeman interaction provides a gap, here the Zeeman interaction is responsible for the crossing at $k = 0$ while spin-orbit interactions open a gap in the spectrum. Due to this gap, the edge-like states are not gappless chiral modes. However, these states (5) exhibit helical electron spin texture similar to the Néel domain walls. We have calculated the texture numerically, Fig.2, taking into account exchange interactions between electrons.

In order to see how non-Abelian quasiparticles can emerge in CdMnTe quantum Hall system, we consider superconductor proximity-induced electron pairing. To illustrate the potential of this system for hosting Majorana modes, we will first assume that the Fermi level

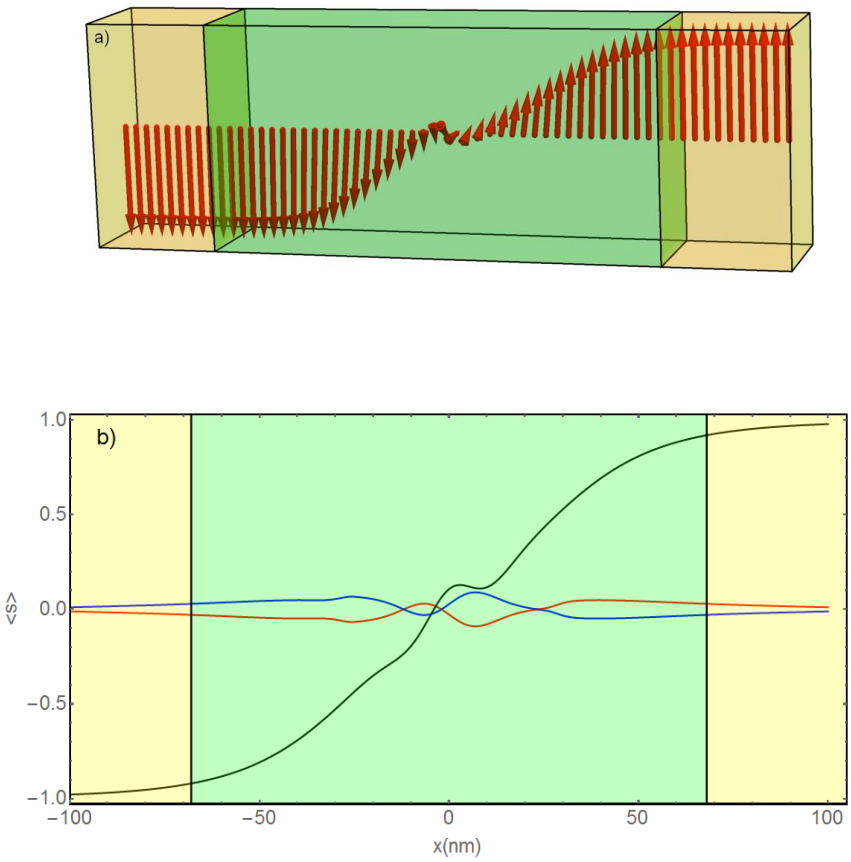

FIG. 2. Panel a) Spin texture as seen by the ground state in a system of two induced edge states originating from LL1 spin down and LL0 spin up states and coupled by Rashba spin-orbit interactions near spectral crossing. Exchange interactions of electrons are taken into account. Gated areas are shown in yellow, while the edge channels are propagating through the green region. Panel b)- Average spin projection on x-direction (blue), $y-direction$ (red) and z-direction (black) directions in the ground state.

is *outside* the spin-orbit gap and crosses edge-like states forming the helical domain wall. The system then is not in the regime of the quantum Hall plateau, presenting difficulties for experimental control, but it is instructive to observe how Majorana modes emerge in this case. The regime of the quantum Hall plateau, when the Fermi level is within the spin-orbit gap in the spectrum of edge states, is considered in the next section.

We assume that the proximity effect is induced by superconducting Ohmic contacts directly coupling edge-like states to an s-wave superconductor. We remark that making such contacts to CdTe directly may be challenging, however, recently Molenkamp group [12]

made superconducting contacts to HgTe, which opens a clear path to achieve contacts by depositing HgTe on CdTe and contacting HgTe. This may present additional important opportunity of controlling proximity superconductivity by voltage applied to the contacts.

Superconducting contacts induce an order parameter $\Delta(x,y)$. Pairing the states of Hamilonian (5) is described by the projected order parameter $\Delta_k = \int dxdy\psi_{0,\downarrow,k_y}\Delta(x)\psi_{1,\uparrow,k_y}$. Due to the opposite velocities of the coupled edge-like states, the Δ_k is sizable even in the approximation of a constant $\Delta(x,y) = \Delta$ despite different Landau indices for the two edges:

$$\Delta_k = \Delta e^{-\frac{m^2\ell^2}{2\hbar^2}v^2}\frac{\sqrt{2}m\ell}{\hbar}v. \tag{6}$$

The corresponding Bogoliubov-de Gennes (BdG) equation $\mathcal{H}\boldsymbol{\psi}(x,y) = E\boldsymbol{\psi}(x,y)$, where $\boldsymbol{\psi}(x,y) = (u_\uparrow, u_\downarrow, v_\downarrow, -v_\uparrow)^T$, is defined by the BdG Hamiltonian

$$\mathcal{H} = \begin{bmatrix} \hbar kv - \mu & h_R & \Delta_k & 0 \\ h_R & -\hbar kv - \mu & 0 & \Delta_k \\ \Delta_k^* & 0 & -\hbar kv + \mu & h_R \\ 0 & \Delta_k^* & h_R & \hbar kv + \mu \end{bmatrix} \tag{7}$$

Its four eigenvalues are:

$$E_k = \pm\sqrt{\Delta_k^2 + \mu^2 + \hbar^2k^2v^2 \pm 2\sqrt{\Delta_k^2h_R^2 + \mu^2h_R^2 + \hbar^2k^2v^2}}\,, \tag{8}$$

where μ is the chemical potential measured from the crossing point energy in the absence of Rashba coupling. The system becomes gapless for $k = 0$ and $\Delta_{k=0}^2 + \mu^2 = h_R^2$, and at $|h_R| < \sqrt{\Delta_{k=0}^2 + \mu^2}$, exhibits a topologically non-trivial superconducting phase. Formally, the emergence of a topological superconducting phase is somewhat similar to the case of a topological insulator in proximity to an s-wave superconductor [54], but because it is Zeeman splitting that gives level crossing and spin-orbit interactions that leads to the gap here, the restriction on the topological phase is defined by the value of the spin-orbit coupling rather than by the Zeeman splitting. It is important to notice that for the chemical potential outside the superconducting gap, i.e., $\mu > h_R$, the induced superconducting order is always topological. Furthermore, topological superconductivity exists even in the absence of a spin-orbit coupling at $h_R = 0$. In this case Majorana fermions are localized at the contacts with an s-superconductor at the ends of the domain wall area. This Majorana system can be affected by non-magnetic disorder: in contrast to chiral states (3), eigenstates of Hamiltonian (5)

in the presence of the spin-orbit coupling are subject to backscattering. This is similar to electron scattering off non-magnetic impurities between edge states in topological insulators in the presence of the Zeeman spin splitting in an in-plane magnetic field. Backscattering must lead to reduction of domain wall conductance compared to conductance of domain walls formed by chiral states (3), as supported by experimental data on resistance on the flanks of the quantum Hall $\nu = 2$ plateau in experiments [39]. Thus, for Majorana modes emerging in helical domain wall with the Fermi level positioned outside the spin-orbit gap in the domain wall but inside the quantum Hall gap in the adjacent 2D regions, impurity scattering becomes detrimental in much the same way as for chiral states in semiconductor wires. Majorana fermions are expected to arise only in a very high mobility quantum Hall samples with small impurity scattering. However, even in this case, due to rather narrow interval of energies, 2D bulk regions exhibit finite conduction at the lowest temperatures, complicating the Majorana setting.

For chemical potential μ *inside* the spin-orbit gap, there exists a significant distinction between the present setting and Majorana modes in topological insulators in the presence of Zeeman splitting in an in-plane field. In topological insulators, a superconductor is often assumed to cover the whole area above the edge states at the sample boundary as opposed to a small contact at the side of the domain wall envisioned here. Correspondingly, certain proximity pairing effect exists throughout topological insulator when μ is inside the gap, which is characterized by a trivial superconducting phase. In the present setting, if impurities are not taken into accont, only a very small area defined by a penetration of the wavefunction into an insulating gapped domain wall near the contact would bear some trace of superconductivity, while the rest of the domain wall is generally an insulator. However, as shall see, impurities drastically change this situation.

III. TOPOLOGICAL SUPERCONDUCTIVITY GENERATED BY IMPURITIES

In order to obtain a well-controlled Majorana setting, the electron transport has to be conducted exclusively along the helical domain wall. To achieve this, the quantum Hall ferromagnetic transition should be tuned very close to $\nu = 2$, where the bulk 2D conduction vanishes. In this case μ lays inside the spin-orbit gap and conduction is exponentially suppressed at low temperatures in wide regions. However in short helical domain wall

channels conduction remains finite, and it was concluded that the in-gap impurity states provide the conduction path [39]. We now show that in the presence of superconducting proximity effect, the helical domain walls with in-gap states can be mapped into a modified version of a generalized disordered Kitaev chain [24, 41] where a topologically non-trivial superconducting order and Majorana bound states emerge.

To consider a superconducting proximity effect in the helical domain walls with the Fermi level inside the spin-orbit gap in the spectrum of edge-like states, we first solve a general quantum-mechanical problem of impurity-induced states in a magnetic field in the presence of spin-orbit interactions. We then find impurity states in the domain wall in the presence of the mean field gradient of exchange interactions between electrons and Mn ions J_1. Our goal here is to get analytic results for the impurity-induced states. We first model potential variations from remote ionized impurities as short-range potentials with a bound state energy E_b at zero magnetic field, and solve the system, in which impurity potential is added to Hamiltonian Eq.(1). We then demonstrate that similar results hold when smooth random potential of impurities in the remote doping layer in structures experimentally studied in [37, 39] is modeled by a sum of gaussian potentials.

A. Effect of spin-orbit coupling on Landau level short-range impurity states

Short-range impurities in quantizing magnetic field were considered in [55, 56]. It is convenient to use the following representation for the wavefunctions of an electron in a uniform magnetic field,

$$\psi_{m,n,s}(r,\varphi) = \sqrt{\frac{n!}{(n+m)!2^{m+1}\pi\ell}} e^{\left(im\varphi + \frac{i}{4}\frac{r^2}{\ell^2}\sin(2\varphi) - \frac{r^2}{4\ell^2}\right)} \left(\frac{r}{\ell}\right)^m L_n^m\left(\frac{r^2}{2\ell^2}\right)\chi_s \ , \qquad (9)$$

corresponding to electron states degenerate in m with energy $E^0_{n,m,s} = \hbar\omega_c\left(n+\frac{1}{2}\right) + sV_z$, $s = \pm 1$, V_z is the spin splitting that includes the conduction band Zeeman effect and a mean field exchange splitting due to the electron spin interaction with Mn spins, L_n^m denotes the Laguerre polynomials, r and φ are the polar coordinates, $n \geq 0$ and $m \geq -n$ are integers. In this representation, despite chosen Landau gauge for the magnetic field vector potential (reflected by an asymmetric $\sin 2\varphi$ term in the exponent), the electron wavefunctions are localized and normalized to unity, and energy levels are multiply degenerate in quantum number m. While in this gauge, due to $\sin 2\varphi$ term in the exponent, the quantum number

m does not have a precise meaning of the electron angular momentum, we will still loosely use the term angular momentum for m. As it is well-known, it is possible to choose a linear combination of these wavefunctions, which would be delocalized. Importantly, in the presence of the in-plane electric field these states are no longer degenerate and describe a drift of the guiding centers in the direction perpendicular to both an electric and a magnetic field. Similarly, propagating edge states can be formed.

Following [55, 56] we begin with considering a single impurity at the origin in the presence of the Landau quantization. The short-range impurity does not affect states with $m \neq 0$ as their wavefunction is zero in the origin, and all states with $m \neq 0$ are still described by the wavefunctions given by Eq. (9) and the corresponding eigenenergies $E^0_{m\neq 0,n,s}$. The states with $m = 0$ are bounded by the impurity and the energy and wavefunctions of these states are:

$$E^i_{0,n,s} = \hbar\omega_c \left(n + \frac{1}{2} - \delta_n \right) + sV_z \tag{10}$$

$$\psi^i_{0,n,s} = \frac{|\Gamma(-n+\delta_n)|}{\sqrt{\pi \Psi'(-n+\delta_n)}} \frac{(-1)^n}{r} e^{\frac{ir^2 \sin(2\phi)}{4}} W_{n+\frac{1}{2}-\delta_n,0}\left(\frac{r^2}{2}\right) \chi_s \ , \tag{11}$$

where W is the Whittaker function and Ψ is the digamma function. In a high magnetic field limit the impurity split-off δ_n is given by

$$\delta_n = \left| \Psi(n+1) - \ln \frac{|E_b|}{\hbar\omega_c} \right|^{-1} \ , \tag{12}$$

For states with $\delta_n \ll 1$ the digamma function in Eq. (12) is much smaller than the logarithmic part and $\delta_n = 1/\ln(\hbar\omega_c/|E_b|) \equiv \delta$ is independent of n. To simplify our analysis, we will consider this approximation; our conclusions, however, are quite general and this restriction is not crucial.

We now include the Rashba Hamiltonian H_R using the basis set that includes the orthonormalized wavefunctions Eq. (9) for $m \neq 0$ and wavefunction determined by Eq. (10) for $m = 0$. The non-zero matrix elements are

$$\begin{aligned} \langle \psi_{m-1,n,\uparrow} | \, H_R \, | \psi_{m,n-1,\downarrow} \rangle &= \tfrac{\beta\sqrt{2n}}{\ell} = \Delta_{so}\sqrt{n} \\ \left\langle \psi^i_{0,n,\downarrow} \right| H_R \, | \psi_{-1,n+1,\uparrow} \rangle &\simeq \tfrac{\beta\sqrt{2n}}{\ell} = \Delta_{so}\sqrt{n} \\ \left\langle \psi^i_{0,n,\uparrow} \right| H_R \, | \psi_{1,n-1,\downarrow} \rangle &\simeq \tfrac{\beta\sqrt{2n}}{\ell} = \Delta_{so}\sqrt{n} \ , \end{aligned} \tag{13}$$

where $\beta = \gamma_R \mathcal{E}_z$. Δ_{so} coinsides with h_R given by Eq. (4) at $n = 1$ when J_1 is neglected, i.e.,

at $v = 0$. Here the matrix elements between Landau level states and impurity states are computed neglecting terms of order of $\mathcal{O}((\beta/\ell)\delta/\hbar\omega_c)$ and $\mathcal{O}(\delta^2)$).

The effect of spin-orbit interaction on Landau electron states and impurity bound states in quantized magnetic field is two-fold. First, $m = 0$ impurity states below the Landau level with index n and spin up couple to pure Landau level $n-1$ spin down states, and similarly $m = 0$ impurity states below the Landau level with index n and spin down couple to pure Landau level $n-1$ spin up states. Coupling of the, e.g., three lowest impurity states are given by

$$\begin{bmatrix} (m,n,s)\backslash(m,n,s) & (0,0,\uparrow)_i & (0,0,\downarrow)_i & (0,1,\uparrow)_i & (1,0,\downarrow)_L & (-1,1,\uparrow)_L \\ (0,0,\uparrow)_i & \frac{\hbar\omega_c}{2} - V_z - \delta & 0 & 0 & 0 & 0 \\ (0,0,\downarrow)_i & 0 & \frac{\hbar\omega_c}{2} + V_z - \delta & 0 & 0 & \Delta_{so} \\ (0,1,\uparrow)_i & 0 & 0 & \frac{3\hbar\omega_c}{2} - V_z - \delta & \Delta_{so} & 0 \\ (1,0,\downarrow)_L & 0 & 0 & \Delta_{so} & \frac{\hbar\omega_c}{2} + V_z & 0 \\ (-1,1,\uparrow)_L & 0 & \Delta_{so} & 0 & 0 & \frac{3\hbar\omega_c}{2} - V_z \end{bmatrix} \tag{14}$$

The impurity state $m = 0$, $n = 0$ and spin up does not couple to any state. In (14) the wavefunctions $(0,n,\uparrow)_i = \psi^i_{0,n,-1}$ and $(0,0,\downarrow)_i = \psi^i_{0,0,1}$ are defined by Eq. (10), and the wavefunctionss $(-1,n,\uparrow)_L = \psi_{-1,n,-1}$ and $(1,n,\downarrow)_L = \psi_{1,n,1}$ are defined by Eq. (9). We underscore the origin of coupling states by using subscript i for $m = 0$ impurity states and subscript L for $m \neq 0$ pure Landau level states in the absence of spin-orbit interactions. Similarly to the lowest states in Eq. (14), unbound and impurity-bound states in higher Landau levels form two-level systems: due to spin-orbit interactions any impurity-bound state couples to a single pure Landau level state (with $m = 1$ or $m = -1$ depending on the spin of the coupled $m = 0$ state), and splits the $m = 1$ or $m = -1$ state off the Landau level, resulting in the two series of impurity states:

$$E^+_{n,\varsigma} = \hbar\omega_c\left(n - \frac{\delta}{2}\right) + \varsigma\sqrt{\left(\hbar\omega_c\frac{1-\delta}{2} - V_z\right)^2 + n\Delta^2_{so}}\,, \tag{15}$$

$$E^-_{n,\varsigma} = \hbar\omega_c\left(n - \frac{\delta}{2}\right) + \varsigma\sqrt{\left(\hbar\omega_c\frac{1+\delta}{2} - V_z\right)^2 + n\Delta^2_{so}}\,, \tag{16}$$

where $(n \geq 1)$, $\varsigma = \pm 1$ denotes two different superpositions of $m = 0$ and $m = -1$ or $m = 0$ and $m = 1$ states for a given n in the corresponding series. Impurity-bound states $E^+_{n,\varsigma}$ originate from $(n-1, m = 1, \downarrow)$ Landau level states in the absence of Rashba interactions,

and states $E^-_{n,\varsigma}$ originate from $(n, m = -1, \uparrow)$ Landau level states in the absence of Rashba interactions. The wavefunctions corresponding to these series of energy levels are given by

$$\psi^+_{n,\varsigma} = \rho^+_+\psi^i_{0,n,-1} + \varsigma\rho^+_-\psi_{1,n-1,1} \tag{17}$$

$$\psi^-_{n,\varsigma} = \rho^-_+\psi^i_{0,n,1} + \varsigma\rho^-_-\psi_{-1,n+1,1}, \tag{18}$$

where

$$\rho^+_+ = \sqrt{\tfrac{1}{2}(1+\gamma_+)}, \quad \rho^+_-= \sqrt{\frac{1}{2}(1-\gamma_+)};$$

$$\rho^-_+ = \sqrt{\tfrac{1}{2}(1+\gamma_-)}, \quad \rho^-_-= \sqrt{\frac{1}{2}(1-\gamma_-)}, \tag{19}$$

$$\gamma_\pm = \frac{\pm\left(\hbar\omega_c\frac{1\mp\delta}{2} - V_z\right)}{\sqrt{\left(\hbar\omega_c\frac{1\mp\delta}{2} - V_z\right)^2 + n\Delta^2_{so}}}. \tag{20}$$

For the remaining $n = 0$ state, which is spin up in a system considered here, the energy and wavefunction of the impurity state are the same as in the absence of spin-orbit interactions and are defined by Eqs. (10, 11). The electron states (15), (16) and impurity state originating from $n = 0$ Landau level do not participate in formation of propagating superposition states in the presence of electric field or near the sample edge, and are bound to impurities.

In order to understand the overall spectrum and hierarchy of electron impurity-bound levels and degenerate Landau levels, we observe that besides the effect of doubling the number of impurity-bound states, the spin-orbit interaction gives an additional repulsion of Landau electron states not bound to impurities, resulting in energy series

$$E_{m,n,s} = \hbar\omega_c n + s\sqrt{n\Delta^2_{so} + \left(\frac{1}{2}\hbar\omega_c - V_z\right)^2} \tag{21}$$

where $s = \pm 1$ and $n \geq 1$. For these states at $s = 1$ the angular momentum $m \neq 1, 0$, and at $s = -1$ the angular momentum $m \neq -1, 0$. All other values of angular momentum in these series characterize degenerate states. The exception is the state with $n = 0$, which is only spin up, and has an energy $E_0 = \hbar\omega_c/2 - V_z$. For this state only $m = 0$ value is excluded from $m-$degenerate states. E_0 is the ground state for $\Delta_{so} \ll \hbar\omega_c$ considered here. Except for the exclusion of states with certain m, Eq. (21) gives the Rashba spectrum for conduction electrons [57]. Energy separation of impurity-unbound levels $\delta E = E_{m,1,+1} - E_{m',1,-1}$ arising from cyclotron splitting as well as spin splitting due to Zeemann, exchange and spin-orbit

interactions, where m and m' characterize degenerate levels for a given value of s, is given by

$$\delta E = 2\sqrt{\Delta_{so}^2 + \left(\frac{1}{2}\hbar\omega_c - V_z\right)^2}. \tag{22}$$

The electron and impurity-bound energy levels in a quantized magnetic field in a quantum well in the presence of the Rashba interactions are shown in Fig. 3. Similar to the spectrum in the absence of Rashba interactions with single $m = 0$ impurity states below each spin-resolved Landau level, here two impurity states (with $m = 0$ and $m = -1$) are below the Landau level wth $s = 1$ and two impurity states (with $m = 0$ and $m = 1$) are below the Landau level wth $s = -1$.

While levels with $m = 0$ are below the corresponding Landau levels in much the same way as their counterparts in the absence of Rashba coupling, spectral positions of $m = 1$ and $m = -1$ impurity-bound levels can be explained by the combined effect of level repulsion due to Δ_{so} and $\hbar\omega_c\delta$, as seen, e.g., from Hamiltonian matrix Eq. (14). The $s = 1$ $m-$degenerate Landau level in the presence of spin-orbit coupling (21) has energy higher than both impurity-bound $E^+_{1,\varsigma=1}$ and $E^-_{1,\varsigma=1}$ states, as can be seen from energy separation between the corresponding levels:

$$E_{m,n=1,+} - E^+_{1,\varsigma=1} = \hbar\omega_c\delta/2 - \sqrt{\left(\hbar\omega_c\tfrac{1-\delta}{2} - V_z\right)^2 + \Delta_{so}^2} + \sqrt{\Delta_{so}^2 + \left(\tfrac{1}{2}\hbar\omega_c - V_z\right)^2}\,, \tag{23}$$

$$E_{m,n=1,+} - E^-_{1,\varsigma=1} = \hbar\omega_c\delta/2 - \sqrt{\left(\hbar\omega_c\tfrac{1+\delta}{2} - V_z\right)^2 + \Delta_{so}^2} + \sqrt{\Delta_{so}^2 + \left(\tfrac{1}{2}\hbar\omega_c - V_z\right)^2}. \tag{24}$$

In the absence of spin-orbit interactions, depending on the sign of $\hbar\omega_c\frac{1-\delta}{2} - V_z$, energy separation described by one of the Eqs. (23,24) is $\hbar\omega_c\delta$, and characterizes the only bound state Eq. (10), while energy separation described by the other of the Eqs. (23,24) vanishes, because no second bound state exists for a given spin-resolved Landau level when spin-oorbit coupling is absent. With an increase of Δ_{so}, e.g., energy separation Eq. (23) decreases, and at large Δ_{so} reaches the value $\hbar\omega_c\delta/2$. In this case energy separation given by Eq. (24) increases, and at large Δ_{so} reaches the same value $\hbar\omega_c\delta/2$ as energy separation Eq. (23). Similarly, the $s = -1$ $m-$degenerate Landau level in the presence of spin-orbit coupling (21) has energy higher than both impurity-bound $E^\pm_{1,\varsigma=-1}$ states. Furthermore, analogous consideration shows that $E_{m,n=1,-}$ state is always lower in energy than states $E^\pm_{1,\varsigma=1}$. Therefore $E^\pm_{1,\varsigma=1}$ states lie between two impurity-unbound levels $E_{m,1,1}$ and $E_{m,1,-1}$ (21), and $E^\pm_{1,\varsigma=-1}$ states are below the $E_{m,1,-1}$ level.

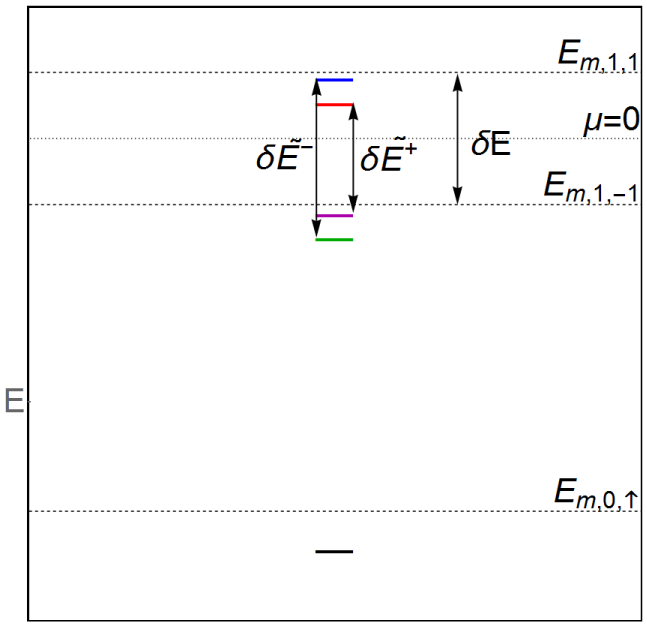

FIG. 3. Electron energy spectrum in quantized magnetic field in the presence of attractive impurity center and spin-orbit interactions in the bulk of the 2D gas. Splitting δE of the degenerate in m and m' $(m, n = 1, s = 1)$ and $(m', n = 1, s = -1)$ levels is given by Eq.(22) and is caused by the cyclotron splitting and spin splitting due to Zeemann, exchange and spin-orbit interactions. Each impurity results in two energy levels for each Landau level, which are given by Eqs. (15) or (16) and are due to either two linear combinations of $m = 0$ and $m = -1$ states for $s = 1$ or two linear combinations of $m = 0$ and $m = 1$ states for $s = -1$. Impurity-bound state $E^-_{1,1}$ is shown in blue, $E^+_{1,1}$ is shown in red, $E^+_{1,-1}$ is shown in magenta and $E^-_{1,-1}$ is shown in green. Splitting of impurity levels $\delta\tilde{E}_+ = E^+_{1,1} - E^+_{1,-1}$ and $\delta\tilde{E}_- = E^-_{1,1} - E^-_{1,-1}$. Due to the effect of split-off $\hbar\omega_c\delta$, $\delta\tilde{E}_- > \delta E > \delta\tilde{E}_+$. Only one impurity induced state, shown in black, arises from $(n = 0, \uparrow)$ Landau level directly above it. These two lowest levels, Landau level and its corresponding impurity-bound state, are not affected by spin-orbit coupling.

At Zeeman energy

$$V_z^* = g\mu_B B + J_0 = \hbar\omega_c/2, \tag{25}$$

energy states $(m, n, s = 1)$ and $(m'n, s = -1)$, and particularly $(m, n = 1, s = 1)$ and $(m', n = 1, s = -1)$ energy states acquire additional double degeneracy in the absence of spin-orbit interactions, but split in its presence, with energies $E_{m,1,\pm1} = \hbar\omega_c \pm \Delta_{so}$.

When condition Eq.(25) is fulfilled, impurity bound states of series with energies $E^+_{n,\varsigma}$

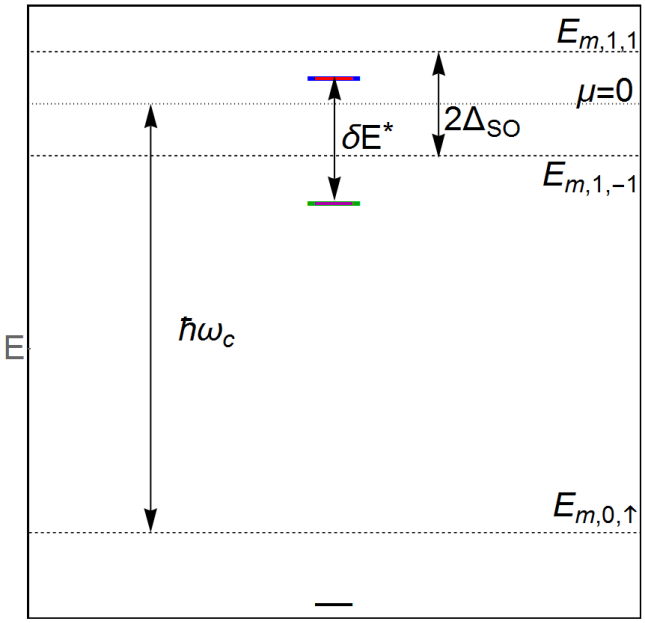

FIG. 4. Electron energy spectrum in quantized magnetic field in the presence of attractive impurity center and spin-orbit interactions in the bulk of the 2D gas in the case of compensation between cyclotron splitting and the sum of the Zeemann and exchange interactions. The splitting $2\Delta_{so}$ of the $(n = 1, s = 1)$ and $(n = 1, s = -1)$ unbound states is due to Rashba coupling only. Impurity levels from $^+$ and $^-$ seriesEqs. (15,16) become degenerate, so that $E^+_{1,1} = E^-_{1,1}$ and $E^+_{1,-1} = E^-_{1,-1}$ (shown as coincidence of blue and red and coincidence of magenta and green). Splitting between pairs of degenerate levels δE^* is due to both Rashba coupling and due to impurity split-off $\hbar\omega_c\delta$.

and $E^-_{n,\varsigma}$ also become degenerate. In particular, as can be shown by considering equations similar to Eqs. (23), (24), the double degenerate level

$$E^*_{n=1,+} = \hbar\omega_c\left(1 - \frac{\delta}{2}\right) + \frac{1}{2}\sqrt{4\Delta^2_{so} + (\hbar\omega_c\delta)^2} \tag{26}$$

corresponding to $\varsigma = 1$ lies in between $(m, n = 1, s = 1)$ and $(m', n = 1, s = -1)$ levels given by Eq. (21), and a double degenerate level at $\varsigma = -1$ with energy

$$E^*_{n=1,-} = \hbar\omega_c(1 - \frac{\delta}{2}) - \frac{1}{2}\sqrt{4\Delta^2_{so} + (\hbar\omega_c\delta)^2} \tag{27}$$

lies below $(m', n = 1, s = -1)$ level. In these equations superscript * corresponds to degeneracy of $^+$ series (15) and $^-$ series, (16). The two degenerate spin-orbit impurity-bound states with energy $E^*_{n,+}$ are orthogonal in spin space, and the two states with energy $E^*_{n=1,-}$

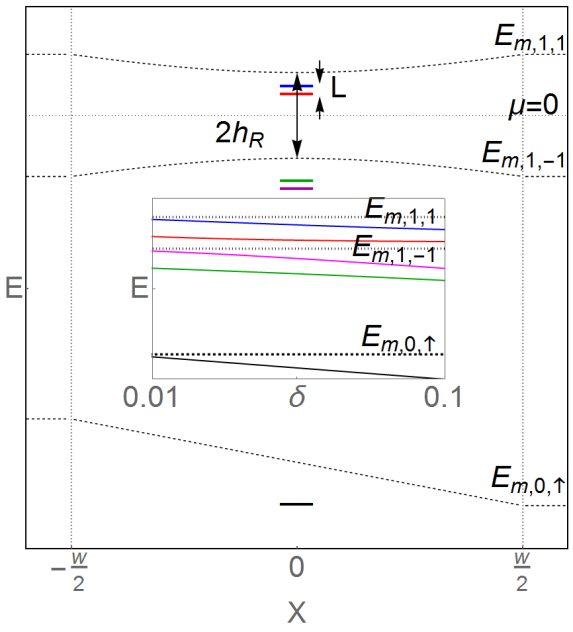

FIG. 5. Electron spectrum in the presence of impurities in a helical domain wall of width W in conditions of compensation between cyclotron energy and the sum of Zeemann and exchange energies for electrons, Eq.(25). The red and blue state doublet are states originating from a double degenerate bulk state $E^*_{n=1,+}$ Eq.(26) of Fig.4 , with a splitting between them due to the gradient of magnetization J_1 according to Eq.(28). The green and and magenta state doublet are states originating from a double degenerate state $E^*_{n=1,-}$ Eq.(27) of Fig.4, with a splitting between them due to the gradient of magnetization J_1 according to Eq.(28). This doublet is below spin-orbit gap. The evolution of splitting of a red-blue and green-magenta doublets are schematically shown in the inset. Electron edge-like states there are also separated by the spin-orbit coupling $2h_R$ in the channel given by Eq. (4). Only a single non-degenerate level (black solid segment) is split off $(m \neq 0, n = 0, \uparrow)$ Landau level shown by the lower black dashed line.

are also orthogonal in spin space. This is a consequence of degeneracy between $(n-1, \uparrow)$ and $(n, \downarrow)$ Landau levels in the case of absence of spin-orbit interactions.

B. Impurity states in a helical domain wall

So far we discussed the Landau levels and the impurity states in the presence of spin-orbit coupling in the "bulk" of the 2D electron liquid . In the presence of the spin-dependent electric field J_1 in a narrow range of coordinate x, which leads to the formation of a helical

domain wall, these states change in a two-fold way. First, Landau levels with multiple degeneracy in angular momenta Eq. (21) form linear combinations that correspond to an edge-like states Eq.(2), which are gapped by spin-orbit interactions and are described by the effective Hamiltonian (5). The two doublets of impurity states also evolve, Fig.5: one doublet with $\varsigma = +1$ falls into the gap between spin-orbit split edge-like states, and the other doublet with $\varsigma = -1$ is below the spin-orbit gap, in accord with their ordering in the 2D bulk, as given by Eqs (15, 16, 21). The second effect of the effective spin-dependent electric field J_1 is angular momentum splitting of the in-gap impurity states. The angular momentum splitting of the $E^*_{1,+}$ double degenerate level (26) for an impurity centered at the origin in the area of the helical domain wall, is given by

$$L = \frac{\hbar^2 v^2}{\ell^2 \sqrt{\left(\hbar\omega_c \delta\right)^2 + 4\Delta_{so}^2}}. \tag{28}$$

Angular momentum splitting L arises in the second order perturbation theory in the effective spin-dependent electric field J_1, and therefore is quadratic in v. The Eq. (28) is valid if the characteristic coupling of impurity state and edge state in the presence of gradient of magnetization $J_1 \ell \ll \hbar\omega_c \delta$. The dependence of angular momentum spliiting of levels on δ is shown in Fig.5, inset. In the experiment [39], the highest $J_1 w \sim 0.07 \hbar\omega_c$, while $w \sim 10\ell$, so $\delta = 0.01$ in the inset of Fig.5 is the lower limit when Eq.(28) can still be applied.

C. Chain of impurity states

Our goal is to study a chain of in-gap states, Fig. 6. For impurity potentials centered at $\mathbf{R}_k = (X_k, Y_k)$, $|R_k - R_{k-1}| \gg \ell$ in high magnetic field, and the dimensions of the chain along the y-direction is much larger than the width of a helical domain wall. Therefore the chain can be considered as one-dimensional, with $\mathbf{R}_k = (X_k = 0, Y_k)$. As we shall see, even when our model will be reduced to a simple model with identical periodically placed impurities, it will show up topological superconductivity and Majorana fermions. However, in order to address a realistic situation that corresponds to quantum Hall structures, we will assume that impurity centers are positioned arbitrarily and may have slightly different binding energies and therefore different impurity split-offs δ. This happens, e.g., because of their varying z-coordinate in a doping layer and therefore varying separation from the quantum well. We will denote the split-off for an impurity centered at $\mathbf{R}_k$ as δ_k. Angular

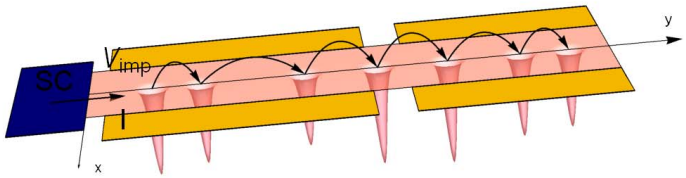

FIG. 6. Schematic view of the conducting channel with proximity induced superconductivity (blue contact), with attractive impurity potential (red)

momentun splittings L_k for impurity sites centered at $\mathbf{R}_k$ also differ from site to site:

$$L_k = \frac{\hbar^2 v^2}{\ell^2 \sqrt{(\hbar\omega_c \delta_k)^2 + 4\Delta_{so}^2}}. \tag{29}$$

The wavefunctions of electrons bound to a single impurity at are given by

$$\psi_m^{(k)}(\mathbf{r}) = \psi_{1,1}^m(\mathbf{r} - \mathbf{R}_k), \tag{30}$$

where $\psi_{1,1}^m(\mathbf{r})$ are defined by Eqs (17), $m = \pm$. To simplify our equations, we will use index m running over $m = 0$ (for + sign) and $m = -1$ (for - sign), so that summation over m will run over $m = 0$ and $m = -1$ states for both directions of spin. We will also drop the Landau level index, because levels under consideration are all characterised by $n = 1$ in the impurity spin-orbit spectrum, Eqs. (15, 16). Considering a chain, we orthogonolize the wavefunctions assuming that only overlap between wavefunctions of electrons centered on the nearest neighbors is essential. The orthonormalized wavefunctions are:

$$\left|\tilde{\psi}_m^{(k)}\right\rangle \simeq \left|\psi_m^{(k)}\right\rangle - \frac{1}{2}\sum_{m_1=-1}^{0} \left|\psi_{m_1}^{(k+1)}\right\rangle S_{m_1,m}^{k+1,k} - \frac{1}{2}\sum_{m_2=-1}^{0} \left|\psi_{m_2}^{(k-1)}\right\rangle S_{m_2,m}^{k-1,k}\ , \quad m = -1, 0\ , \tag{31}$$

where the overlap integrals of the electron wavefunctions on isolated centers located at $\mathbf{R}'_{\mathbf{k}}$ and $\mathbf{R}_{\mathbf{k}}$ are given by

$$S^{k',k}_{m',m} = \left\langle \psi^{k'}_{m'} \middle| \psi^{(k)}_{m} \right\rangle . \tag{32}$$

We seek the wavefunctions of the Hamiltonian of the chain

$$H = -\frac{1}{2m^*}\left(-i\hbar\nabla - \frac{e\mathbf{A}}{c}\right)^2 + V_z\sigma_z + \sum_k U(\mathbf{r}, \mathbf{R}_{\mathbf{k}}) \tag{33}$$

in the form

$$\Psi = \sum_{m,k} a_{mk} \left| \tilde{\psi}^{(k)}_{m} \right\rangle \ , \quad m = -1, 0 \ . \tag{34}$$

Then the effective Hamiltonian $H_{mk,m'k'}$ acting on coefficients a_{mk} is defined by the renormalized single-impurity site energies $\tilde{E_{mk}} = \left\langle \tilde{\psi}^{k}_{m} \middle| H \middle| \tilde{\psi}^{k}_{m} \right\rangle$ and tunneling matrix elements $w^{m',m}_{k',k} = \left\langle \tilde{\psi}^{k'}_{m'} \middle| H \middle| \tilde{\psi}^{k}_{m} \right\rangle$. The leading contribution to tunnelling arises from matrix elements

$$w^{m,m}_{k+1,k} \simeq \tilde{\delta}_{k+1,k}(-1)^{m+1} P_{k+1,k} \frac{1}{4}\left(\frac{Y_{k+1,k}}{\sqrt{2}\ell}\right)^{2m+2} e^{-\frac{Y^2_{k,k+1}}{4\ell^2}} \ , \tag{35}$$

$$w^{-1-m,m}_{k+1,k} \simeq \delta^d_{k+1,k} Q_{k+1,k} \frac{1}{4}\frac{Y_{k+1,k}}{\sqrt{2}\ell} e^{-\frac{Y^2_{k,k+1}}{4\ell^2}} \ , \tag{36}$$

where

$$P_{k+1,k} = 1 - \frac{\hbar\omega_c\tilde{\delta}_{k+1,k}}{\sqrt{(\hbar\omega_c\tilde{\delta}_{k+1,k})^2 + 4\Delta^2_{so}}} \ , \tag{37}$$

$$Q_{k+1,k} = \frac{\Delta_{so}/\sqrt{2}}{\sqrt{(\hbar\omega_c\tilde{\delta}_{k+1,k})^2 + 4\Delta^2_{so}}} \ , \tag{38}$$

$\tilde{\delta}_{k+1,k} = (\delta_k + \delta_{k+1})/2$ is an average split-off of the neighboring impurity centers, $\delta^d_{k+1,k} = \delta_k - \delta_{k+1}$, and $Y_{k+1,k} = Y_{k+1} - Y_k$. These expressions are obtained by expanding the overlap matrix elements and keeping only the leading terms in $1/Y_{k+1,k}$, $e^{-Y^2_{k+1,k}}$ and δ^d.

D. Superconducting coupling

We project electron interactions due to the proximity-induced superconducting paring $H_\Delta = \Delta \int \hat{\psi}^\dagger_\uparrow \hat{\psi}^\dagger_\downarrow + h.c.$, onto the Hilbert space of bound states $\psi^{(k)}_m$. As we are interested here is a single superconducting contact to a quantum Hall system, phase of the order

parameter is unimportant and we take $\Delta > 0$ without the loss of generality. The effective Hamiltonian for the superconducting pairing with a chain of impurity states then reads

$$H_\Delta \simeq \sum_k \tilde{\Delta}_k c^\dagger_{k,0} c^\dagger_{k,-1} + \sum_{m,m'=-1,0} \Delta^{m,m'}_{k,k+1} c^\dagger_{k,m} c^\dagger_{k+1,m'} + h.c. \ , \tag{39}$$

where

$$\tilde{\Delta}_k = \Delta \frac{1-\gamma_0 \delta_k}{\sqrt{8}} \tag{40}$$

$$\Delta^{m,m}_{k,k+1} = \Delta i(4m+3) \left(\frac{Y_{k,k+1}}{\sqrt{2}\ell}\right)^{2m+1} Q_{k+1,k} e^{-\frac{Y^2_{k+1,k}}{8\ell^2}} \tag{41}$$

$$\Delta^{-1-m,m}_{k,k+1} = \Delta(-1)^m(4m+3) \left(\frac{Y_{k,k+1}}{\sqrt{2}\ell}\right)^{2} \left(P_{k+1,k} + m - \frac{1}{2}\right) e^{-\frac{Y^2_{k+1,k}}{8\ell^2}} \ , \tag{42}$$

$\gamma_0 \simeq 1.89258$ is a numerical constant, and $m = -1, 0$, $c^\dagger_{k,m}$ and $c_{k,m}$ are creation and annihilation operators for electrons in state $|\psi^k_m>$.

E. Single impurity site in the presence of superconducting pairing

In order to address the topological superconductivity and Majorana fermions in a chain of impurity states, we first consider a single site in the presence of superconducting coupling within the Bogoliubov-DeGennes formalism. We restrict the Hilbert space to $\psi^1_{1,0,-1}$ and $\psi^1_{1,-1,-1}$ near impurity site k with coordinates R_k. We denote electron creation operators for these states $c^\dagger_{k,+1}$ and $c^\dagger_{k,-1}$. Then the effective Hamiltonian is given by

$$H_k = \sum_{i,j} \left(\varepsilon_k + L_k \sigma_z\right)_{i,j} c^\dagger_{k,i} c_{k,j} + i\tilde{\Delta}_k \hat{c}^\dagger_{k,i} \left(\sigma_y\right)_{i,j} \hat{c}^\dagger_{k,j} - i\tilde{\Delta}_k \hat{c}_{k,i} \left(\sigma_y\right)_{i,j} \hat{c}_{k,j} \ , \tag{43}$$

where μ is the chemical potential, and on-site energies are

$$\varepsilon_k = -\hbar\omega_c \frac{\delta_k}{2} + \frac{1}{2}\sqrt{\left(\hbar\omega_c\delta_k\right)^2 + 4\Delta^2_{so}} - \mu \ , \tag{44}$$

where $\tilde{\Delta}_k$ is defined by Eq. (40). We diagonalize this Hamiltonian using the Bogoliubov transformation

$$\hat{a}_{k,\pm} = \pm \sqrt{1 + \frac{\varepsilon_k}{\sqrt{\varepsilon^2_k + |\tilde{\Delta}_k|^2}}} e^{i\frac{\pi}{4}} \hat{c}_{k,\pm 1} + \sqrt{1 - \frac{\varepsilon_k}{\sqrt{\varepsilon^2_k + |\tilde{\Delta}_k|^2}}} e^{i\frac{\pi}{4}} c^\dagger_{k,\mp 1} \tag{45}$$

that gives eigenvalues $\mu_k \pm L_k$, where

$$\mu_k = \sqrt{\tilde{\Delta}^2_k + \epsilon^2_k}. \tag{46}$$

F. Topological superconductivity in a chain of impurity-bound states

We now study a chain of impurity-bound sites placed at $\mathbf{R}_k = (0, Y_k)$. We denote $\mathbf{R}_{k,k+1} = \mathbf{R}_{k+1} - \mathbf{R}_k$. The Hamiltonian of the chain is defined by the single site energies, superconducting coupling and inter-site tunneling:

$$H_c = \sum_k H_k + \sum_{k,i,j} w^{i,j}_{k+1,k} \hat{c}^\dagger_{k+1,i} \hat{c}_{k,j} + \sum_{k,i,j} \Delta^{i,j}_{k+1,k} c^\dagger_{k+1,i} \hat{c}^\dagger_{k,j} + h.c \ , \tag{47}$$

where $w^{i,j}_{k+1,k}$ are given by Eqs. (35), (36) and $\Delta^{i,j}_{k+1,k}$ are given by Eqs. (41) and (42). Analogous to [25], we project the Hamiltonian H_c onto the subspace of fermionic excitations given by $a_{k,-}$ on each site. These excitations are defined by Eq.(45). Then the effective Hamiltonian is

$$H = \sum_k \left[(\mu_k - L_k)\, \hat{a}^\dagger_{k,-} \hat{a}_{k,-} + t_k \hat{a}^\dagger_{k+1,-} \hat{a}_{k,-} + \bar{\Delta}_k \hat{a}^\dagger_{k+1,-} \hat{a}^\dagger_{k,-} \right] + h.c. \ , \tag{48}$$

where in the leading approximation

$$t_{k,k+1} = \Delta \frac{\sqrt{2}}{4} \left(\frac{Y_{k+1,k}}{\sqrt{2}\ell} \right)^2 r_{k,\delta} \sqrt{1 + r^2_{k,\delta}} \left(P_{k+1,k} - \frac{3}{4} \right) e^{-\frac{Y^2_{k+1,k}}{8\ell^2}} \ , \tag{49}$$

$$\bar{\Delta}_{k,k+1} = \Delta \frac{3}{16} \left(\frac{Y_{k+1,k}}{\sqrt{2}\ell} \right)^3 \sqrt{1 + r^2_{k,\delta}} \left(\sqrt{1 + r^2_{k,\delta}} - 1 \right) Q_{k+1,k} e^{-\frac{Y^2_{k+1,k}}{8\ell^2}} \ , \tag{50}$$

$\mu_{k+1,k} = (\mu_k + \mu_{k+1})/2$ and $r_{k,\delta} = \tilde{\Delta}/\mu_{k+1,k}$.

The term proportional to $\bar{\Delta}_{k,k+1}$ constitutes a p-type superconducting pairing. We therefore arrived at the Hamiltonian similar to that of a generalized version [24, 25] of the Kitaev chain [41]. However, due to different symmetry of our system, angular momentum splittings L_k are defined by gate voltages. Except possibly for the $\left(P_{k+1,k} - \frac{3}{4}\right)$ factors appearing in the definition of an effective tunneling amplitudes $t_{k,k+1}$, and a superconducting pairing $\bar{\Delta}_{k,k+1}$ do not change sign from site to site. From Eq. (37), $t_{k,k+1}$ becomes zero when $\hbar\omega_c \delta_k = 2\Delta_{so}\sqrt{1/15}$. The task is then to adjust chemical potential μ so that either $t_{k,k+1} > 0$ or $t_{k,k+1} < 0$ throughout the chain of impurity sites. Positioning μ via slight tuning of front or back gate, we can choose a strip of states with sufficiently small short range potential amplitudes δ_k and δ_{k+1}, close to the bottom of the upper hybridized state of the Hamiltonian (5), making all factors $P_{k+1,k} - 3/4$ positive, or impurity states approximately below the middle of the spin-orbit gap, when all these factors become negative. We note that the need for the factor $P_{k+1,k} - 3/4$ to maintain the same sign from site to site is a feature

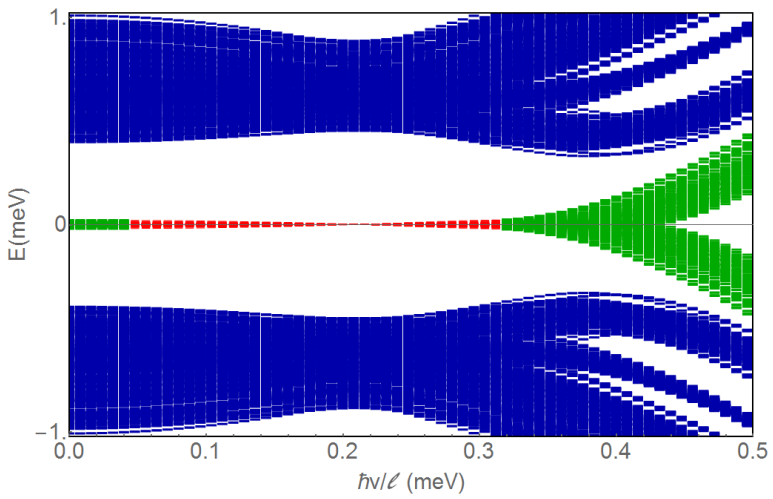

FIG. 7. Spectra of 100 realizations of a chain of 5 localized states with superconducting coupling. The total length of the chain is 200 nm. Bound states energies $\in [\mu - k_BT, \mu + k_BT]$, where $T = 0.1$K. Minimal separation of centers of localized states is 25 nm, $\Delta = 0.1$meV, $\gamma_R = 0.44$meVnm $\mu = 32\mu$eV. In-gap states that disappear with increasing velocity or at small velocities (transitions from red to green) signify the existence of the Majorana bound states (red).

needed in the case of impurity potential being indeed sufficiently random. For the model of identical periodically placed impurities, this condition is fulfilled automatically. It is also fulfilled when impurities have close δ_k, which is most likely in experimental conditions.

We thus arrive to the setting analogous to a sign ordered Kitaev chain [24] that supports two Majorana localized modes at its ends if

$$|\mu_k - L_k| < \max(t_{k,k+1}, \bar{\Delta}_{k,k+1}). \tag{51}$$

Although this criterion creates an impression that it can possibly be satisfied even at $L_k = 0$, it is important to keep in mind that non-zero $L_k > k_BT$ is an important factor that prevents fermion doubling. L_k separates two angular momentum/spin species of in-gap states proximity-coupled to a superconductor. That constitutes a difference between the setting of in-gap Majorana modes and Majorana modes in a topological insulator. In a topological insulator proximity-coupled to a superconductor, Majorana modes can emerge at zero Zeeman splitting because fermion doubling in topological insulator is removed by the chiral character of spin edge states. However, the in-gap electron states in our setting do not propagate, and are not characterized by a wavevector. In the absence of J_1 defining the velocity v of the edge states, the impurity states are degenerate in angular momentum

and spin simultaneously, which leads to the fermion doubling. That would be the property of impurity states in spin-orbit gap emerging at a virtual crossing of 2D bulk Landau levels in conditions (25), which cannot be used for Majorana modes in contrast to impurity states in edge spectrum. For these impurity states in the gap at the domain wall, the gradient of exchange interactions results in angular momentum splitting L_k that removes fermion doubling, and leads to the emergence of topological superconductivity. We observe that the symmetry of the emerging analog of Kitaev chain differs from that in [24]. The primary source of difference is that our system originates from helical states, for which the topological criterion is that spin-orbit gap must be smaller than superconducting gap. In the chain, we have small L_k splitting due to difference of gate voltage that induces the domain wall. In contrast, the chain of quantum dots in [24] was considered at large Zeeman splitting echoing the criterion of topological superconductivity for Rashba wires, in which Zeeman slitting must exceed the spin-orbit gap. We shall see that in a disordered chain, the possibility of small splittings L_k of on-site energies results in the appearance of additional range of normal induced superconductivity in the domain wall area, and the corresponding phase transition between normal and topological phases.

In Fig. 7, we present numerically calculated spectra of a short chain of localized states with proximity-induced superconducting coupling depending on the difference of gate voltages creating the domain wall. It is convenient to characterize this difference by the parameter describing the velocity of counterpropagating edge-like channels v, proportional to J_1. Choosing binding energies of impurities to be sufficiently random, with positive μ_k given by Eq. (46) satisfying $\mu_k > \max(t_{k,k+1}, \bar{\Delta}_{k,k+1})$, we find that at small velocities and therefore small L_k, the chain is in a trivial superconducting state. With increasing J_1, and increasing L_k, the absolute value of the difference $|\mu_k - L_k|$ decreases and Majorana modes and topological superconductivity emerges at $|\mu_k - L_k| < \max(t_{k,k+1}, \bar{\Delta}_{k,k+1})$. At yet higher L_k we again return to $|\mu_k - L_k| > \max(t_{k,k+1}, \bar{\Delta}_{k,k+1})$ and trivial superconducting order. We note that for almost identical periodical placed impurities, the range of topological superconductivity extends to smallest v, with the only condition that J_1 is sufficient to create the domain wall area itself, i.e., $J_1 w > \hbar/\tau$, where $\hbar/\tau$ is the Landau level broadening. We estimate that in conditions of experiment [39], $J_1 w \sim 0.07\hbar\omega_c$. The high v range of normal superconductor is practically the same for random or identical impurities, and is defined primarily by the characteristic value of L_k. The condition for the topological phase transition between normal

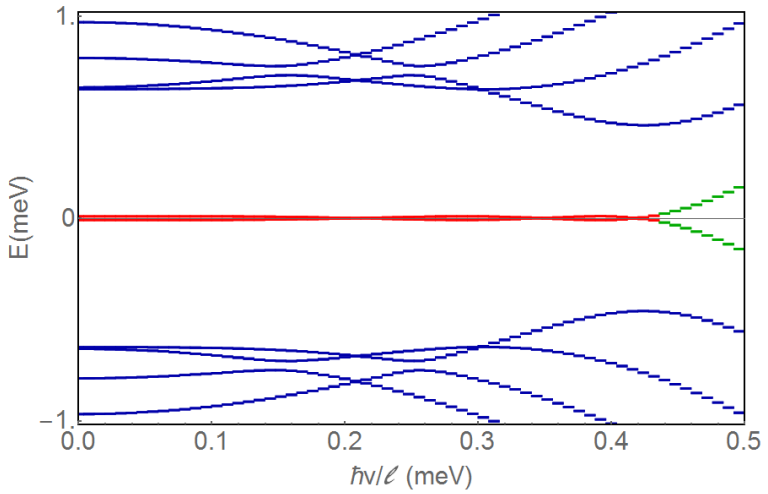

FIG. 8. Energy spectrum of 5 idential localized states separated by 40 nm, with binding energy 48 μeV at chemical potential $\mu = 32\mu eV$ In contrast to randomly placed impurities this regular chain leads to a phase diagram with one range of parameters with topological superconducting order followed by the range with conventional superconducting order.

and topological order at high v corresponds to $\hbar v/\ell \approx 0.3$. The condition for the topological phase transition between normal and topological order at low v corresponds to $\hbar v/\ell \approx 0.04$.

Thus, tuning the angular momentum splitting L_k, which is achieved by tuning the difference of gate voltages V on the left and the right top gates, and in turn strongly tunes the gradient of magnetization J_1, we can bring the system in and out of the topological phase, creating and destroying Majorana modes at the end of the chain. L_k, in contrast to settings described in [24, 25] is unrelated to the value of a magnetic field, but is defined by velocities of gapped edge channels v, which are controlled by electrostatic gates. We also note that other quantities, i.e. μ_k, t_k and $\bar{\Delta}_k$ defined by Eqs. (35-42) are not proportional to the gate voltage difference V in the case of the impurity chain, and essentially do not depend on it.

We conclude the discussion of the short-range potential case by presenting a phase diagram for the case of identical equally spaced impurities, shown in Fig.8. In this case, fluctuations in chemical potential of the impurity sites are absent, when splitting L is larger than tunneling and superconducting gap amplitudes the system exhibits conventional superconductivity, and small L leads to topological superconducting order. Then the phase diagram is the same as Kitaev's and as the case of large Zeeman splitting in disordered chain considered in [24].

G. Topological superconductivity and Majorana fermions in the presence of a smooth random potential

So far we modeled disorder as a short-range potential. In the case of heterostructures studied experimentally in [37, 39], the character of potential is probably intermediate between smooth random potential and a short range-disorder. Even if we imagine that only smooth random potential is present, the experimental picture of conductance in the system is expected to be similar to what is observed in [37, 39]: a peak of conductance tunable throughout the quantum Hall plateau, which is not overshadowed by a thermally activated conductance through the 2D bulk. The conductance peak should be also clearly separated from conductance through propagating chiral edge states. This means that smooth random potential profile also must provide conducting channels through the spin-orbit gap in order to result in an experimentally observed conductance signal. In this subsection we consider Majorana fermions emerging in the case of a model describing a smooth random potential.

We model a smooth ransom potential as a sum of Gaussians

$$V(r) = -\sum_k v_k e^{-\frac{(\mathbf{r}-\mathbf{R}_k)^2}{2r_k^2}} \ . \tag{52}$$

The Gaussians, Fig. 9 are centered around points that are in the middle of the channel $\mathbf{R}_k = (0, Y_k)$. In this model the potentials $v_k \ll \hbar\omega_c$ and radii of the potential $r_k \gg \ell$. In this model, bound states are formed near the minima and the electrons can tunnel under the saddle point potentials. We find that these bound states are important for Majorana physics.

In order to see an analogy between short-range and a collection of gaussians potentials, we consider a single particle model for one Gaussian potential minimum. In the presence of a Zeeman term at degeneracy condition (25) $V_z^* = \hbar\omega_c/2$ the energy levels and eigenfunctions are as follows:

$$E_{m,n,\varsigma} \approx \hbar\omega_c n - v_0 + \frac{v_0\ell^2}{r_0^2}\left(2n + \frac{3}{2} + m\right) + \frac{\varsigma}{2}\sqrt{\frac{v_0^2\ell^4}{r_0^4} + 4n\Delta_{so}^2} \ , \tag{53}$$

$$\psi^s_{m,n,\varsigma} = \frac{1}{\sqrt{2}}\left(\sqrt{1 + \frac{v_0}{\sqrt{\frac{v_0^2\ell^4}{r_0^4} + 4n\Delta_{so}^2}}}\psi_{m,n,1} - \varsigma\sqrt{1 - \frac{v_0}{\sqrt{\frac{v_0^2\ell^4}{r_0^4} + 4n\Delta_{so}^2}}}\psi_{m+1,n-1,-1}\right) \tag{54}$$

where $\varsigma = \pm 1$. This expressions have been obtained by retaining only linear terms in v_0 and $1/r_0^2$. Levels $\psi^s_{m,n,1}$ and $\psi^s_{m+1,n,-1}$ are degenerate when (25) holds, similarly to the

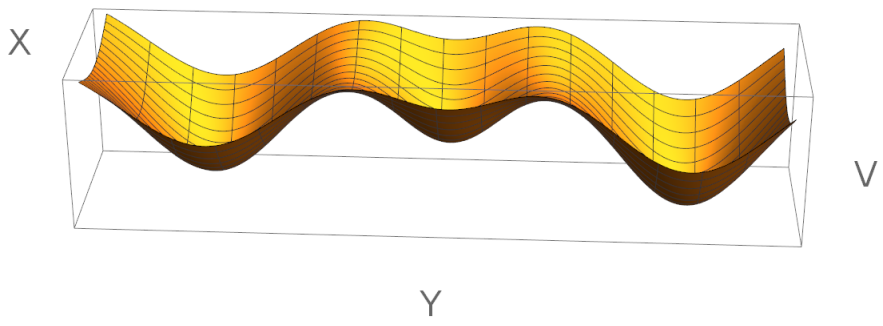

FIG. 9. Model smooth random potential. In this fragment of a smooth random potential, three gaussians result in three potential wells and two saddle points.

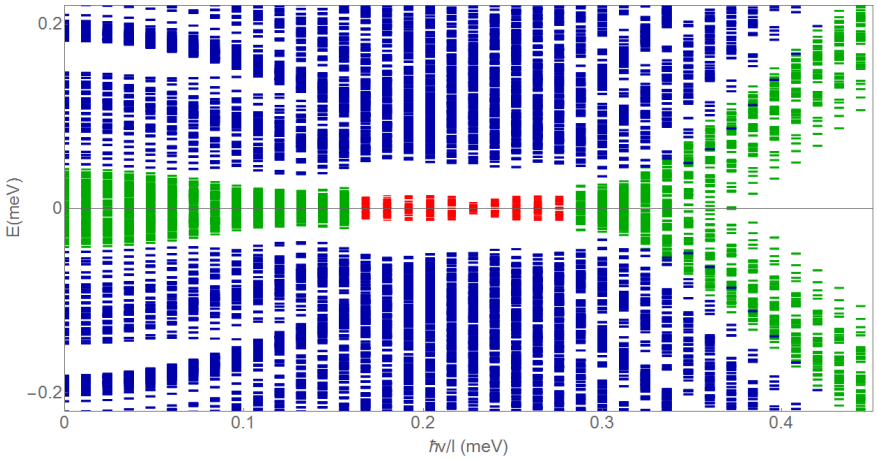

FIG. 10. Spectra of 100 realizations of a chain with 5 gaussian potentials in Eq. (52) with localized states and tunneling and superconducting coupling. The total length of the chain is 200 nm. Bound states energies $\in [\mu - k_B T, \mu + k_B T]$, where $T = 0.1$K. $\Delta = 0.1$meV, $\gamma_R = 0.44$meVnm $\mu = 32\mu$eV, potential amplitudes are less than 0.8meV and radii 40nm $\leq r_k \leq$ 50nm.

short-range potential spectra Eq. (26). Comparing the cases of gaussian potential and short-range potential, we observe that $v_0\ell^2/r_0^2$ plays the role of splitting between impurity level and degenerate Landau level $\hbar\omega_c\delta$. Position-dependent magnetization term proportional to J_1, i.e., to the spin-dependent electric field, leads to splitting of the spin-degenerate levels Eq. (53), resulting in quadratic in J_1 splitting L_k^s analogous to L_k defined by Eq. (29).

The procedure for considering the topological superconductivity and Majorana fermions is similar the case of $\delta-$potential. We start with two bound levels with energy separation L_k^s at each minima, orthogonalize them by taking into account overlaps with their nearest neighbors and compute tunneling and superconducting proximity order parameter matrix elements. We then solve the on-site Bogoliubov-de Gennes equations and use these solutions as a basis set for the effective Hamiltonian describing coupling between neighboring potential minima. Similarly to the case of a short-range potential, we arrive to the modified generalized Kitaev chain with parameters describing tunneling $t_{k,k+1}^s$ and superconducting proximity order parameter $\bar{\Delta}_{k,k+1}^s$ matrix elements, where superscript s distinguishes these quantities in the case of smooth random potential from the similar quantities for a short range potential. The symmetry of the chain is defined by angular momentum splitting L_k^s controlled electrostatically. The generalized Kitaev chain exhibits topological superconductivity and Majorana zero modes when the condition $|\mu_k - L_k^s| < \max(t_{k,k+1}^s, \bar{\Delta}_{k,k+1}^s)$, the same as the criterion (51) for the short-range potential, is satisfied.

Numerical simulations were performed for heterostructures studied in [39] assuming $\Delta =$ 0.1 meV, $\gamma_R = 0.44$ meV·nm, and $\mu = 32$ μeV . Similarly to the case of a short-range potential, Fig. 10 exhibits two ranges with conventional proximity-induced superconductivity and a range with topological superconductivity in between the normal ranges, depending on the difference of gate voltages defining the domain wall. Numerics shows that compared to the model of short range potentials, the range of topological superconducting phase is narrower, but nevertheless clearly manifests itself.

H. Majorana fermions

I. Control of Majorana modes

We will analyze manipulation of the Majorana modes using an example of the system of short-range potential with the phase diagram shown on Fig. 7. We estimate that the voltage difference between the gates $V = V_1 - V_2 \sim 129$ mV corresponds to the topological condition $\hbar v/\ell < 0.3$ with Majorana fermions formed at the end of the chain, while additional voltage $\delta V \sim 1$ mV (total voltage difference $V + \delta V$) brings the system to the normal superconducting proximity state.

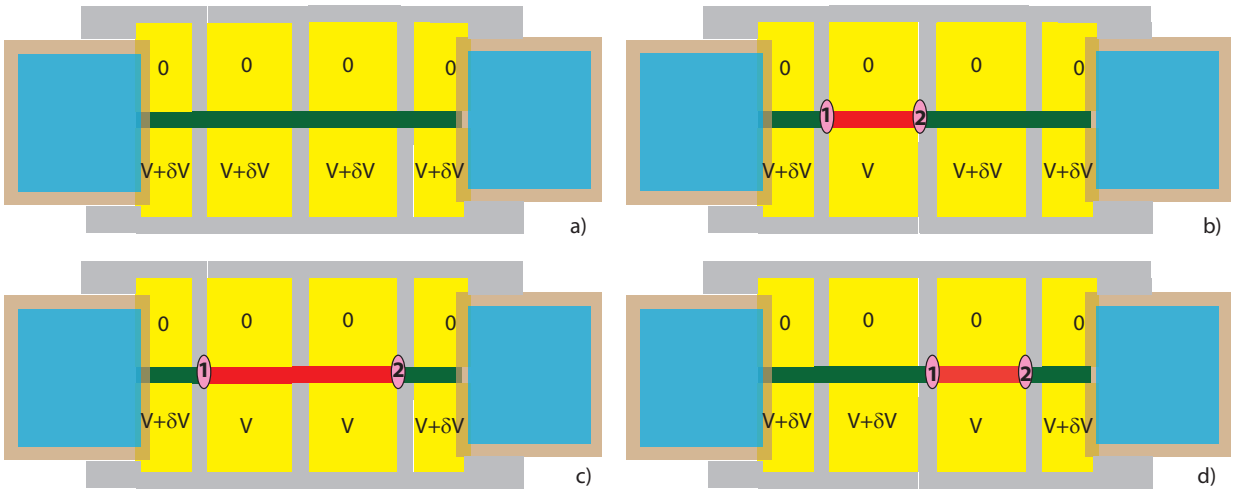

FIG. 11. Creating and moving a Majorana pair: a) Setting voltage differences between top and bottom gates to $V + \delta V$ yields trivial superconductivity in all domain walls; b) setting voltage to V on the second bottom gate drives the system into the topological phase in the domain wall above that gate and induces the Majorana modes at the ends of the domain wall; c) Setting the voltage to V on the third bottom gate extends the topological region to the domain wall above that gate and moves one of the Majorana modes to a new boundary between topological and non-topological state; d) Setting the voltage to $V + \delta V$ on the second bottom gate moves the first of Majorana modes to the right. Blue areas are s-superconductors, yellow areas are top gates. Difference of voltages between two neighboring yellow gates defines the presence of domain wall and the type of the superconducting order parameter. Red domain walls are in topological superconducting state, and green domain walls are non-topological superconductors. Grey areas correspond to voltage differences between neighboring gates insufficient to create a domain wall.

Thus, using electrostatic gates, we can move Majorana modes, and create and annihilate them. Furthermore, reduction of the difference of voltages on electrostatic gates on the sides of the domain wall area to a voltage below 10 meV (in theory, making it zero) erases the domain wall altogether, and can also serve as an instrument in manipulating reconfigurable network of topological superconductors. Figs. 11, 12, 13 and 14 demonstrate inducing, moving, exchange, fusion and braiding of Majorana modes. In these figures, blue areas are s-superconductors and yellow areas are top gates. Difference of voltages between two neighboring yellow gates defines the presence of domain wall and the type of the superconducting order parameter. Red domain walls are in topological superconducting state,

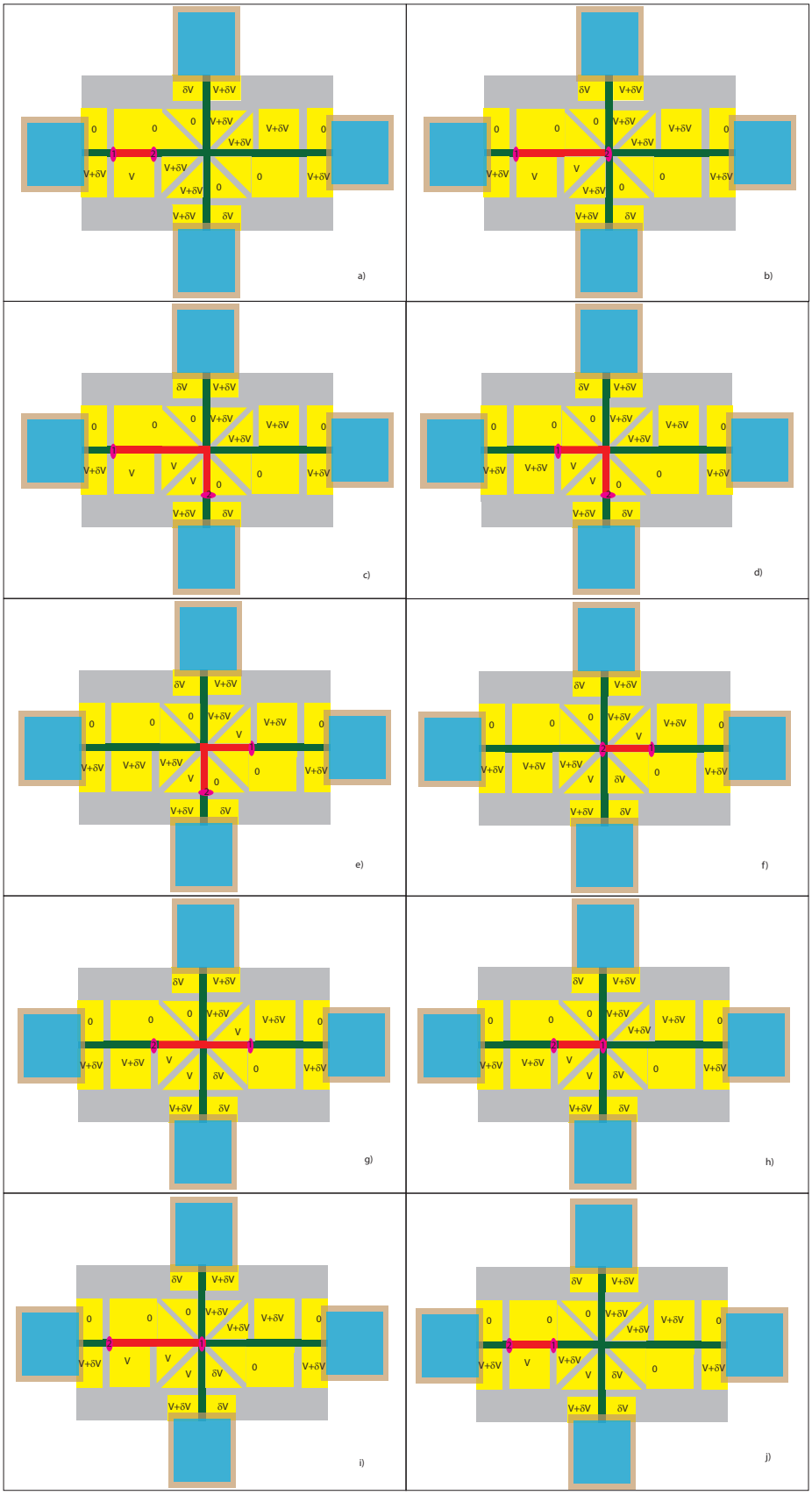

FIG. 12. Exchanging a pair of Majorana modes using method of moving the Majorana pair.

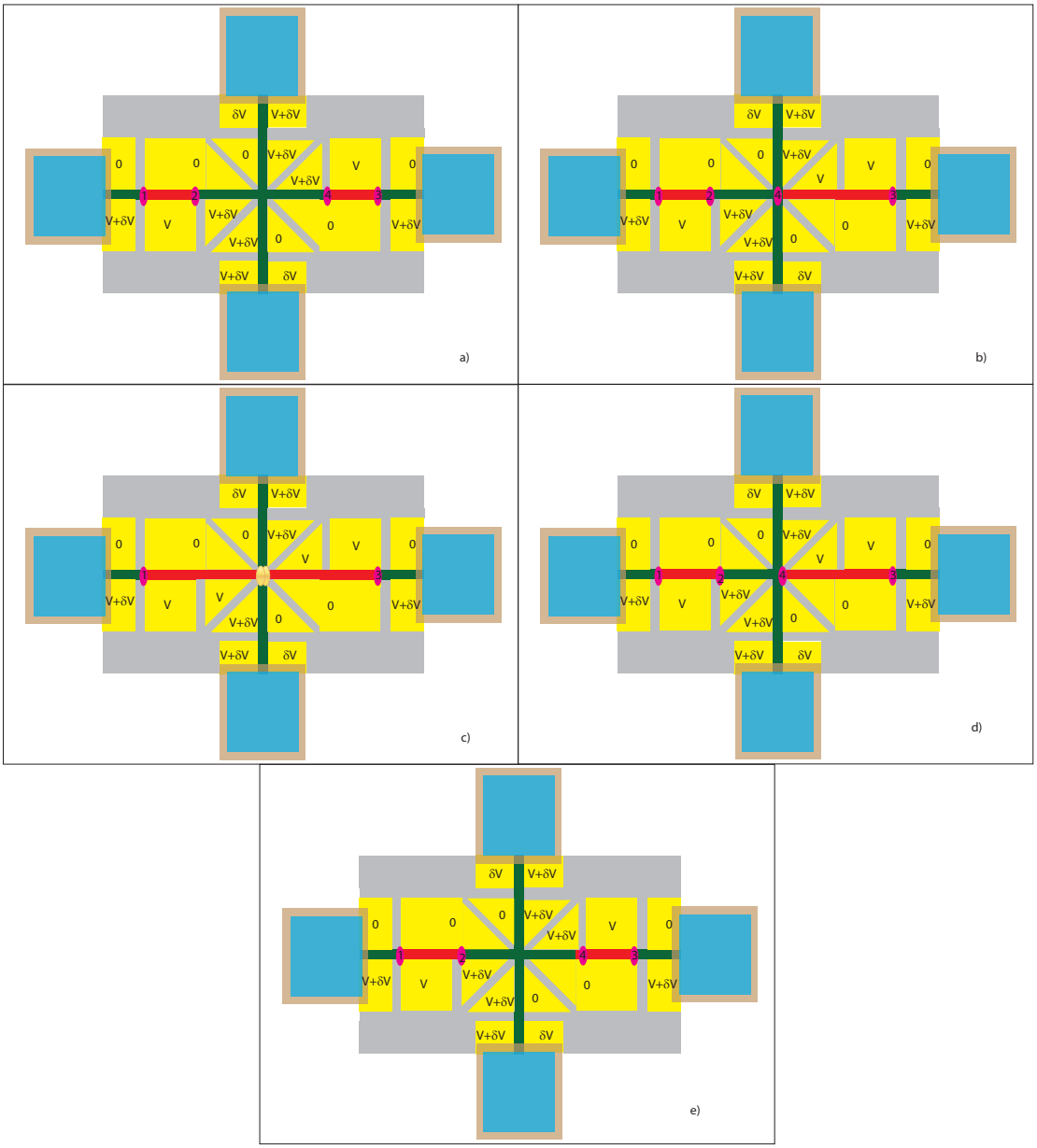

FIG. 13. Fusion and recreation of Majorana modes using method of moving the Majorana pair.

and green domain walls are non-topological superconductors, while grey areas correspond to voltage differences between neighboring gates insufficient to create a domain wall. Braiding of Majorana fermions are achieved using a structure containing T-junction of domain walls in topological superconducting state, Fig. 14. By moving Majorana modes, two pairs of such modes are brought to a T-junction as in panel d). Then a T-junction link is cut by increasing the voltage by δV on the gate controlling that link. Gate voltages are then brought back to the initial configuration. We underscore that all manipulations are expected to be

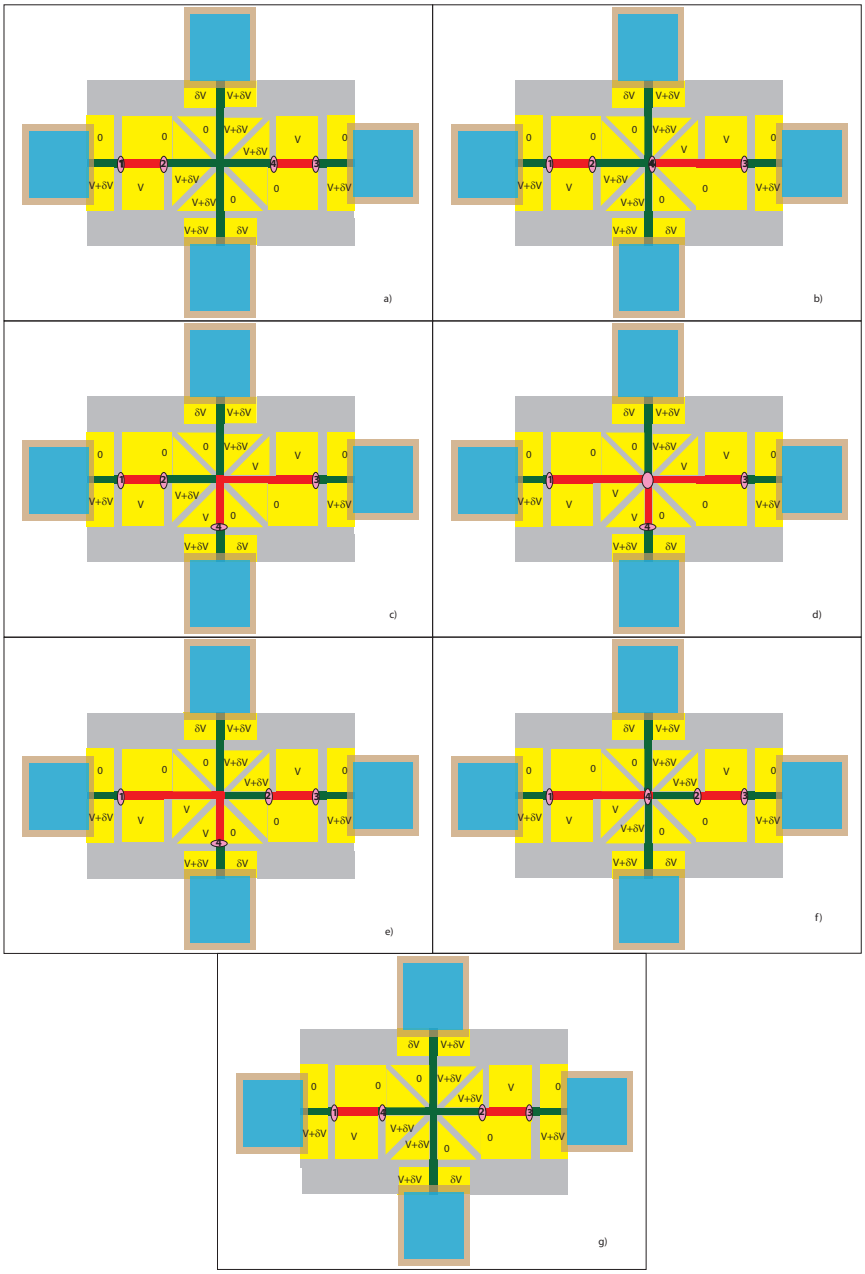

FIG. 14. Braiding Majorana modes achieved using a method of moving the Majorana pair and a T-junction of domain walls in topological superconducting state.

produced by voltage pulses. Calculated parameters and requirements for the scheme are realistic and feasible for experiments in near future.

We note that in the schemes Fig.11-14, a superconducting pairing potential Δ is assumed spatially uniform in the domain wall areas. In real settings with superconducting contacts on the sides of the domain walls, the induced superconducting gap is expected to be spatially

dependent, decreasing from the contact area into the sample. Spatially dependent $\Delta(y)$ will re-define boundaries between topological and non-topological superconducting regions. These boundaries, and Majorana modes residing at boundaries, can be moved with adjusted gate voltages, when applied gate voltage exceeds the critical value in an area with lower Δ but is smaller than the critical value in the area closer to the contact.

IV. CONCLUSION

In this work we considered Majorana modes in hybrid s-superconductor - filling factor $\nu = 2$ quantum Hall ferromagnet domain wall system. We discovered that when the Fermi level is pinned to a gap between anticrossing spin-orbit coupled edge states, the impurity disorder in short domain walls generates proximity-induced topological superconductivity and the Majorana zero modes. Thus, in this case not only topological superconductivity is disorder robust, but it emerges exclusively due to impurities. For sufficient impurity randomness, the phase diagram shows two ranges of gate voltage with conventional superconducting order, separated by a range with topological superconductivity. Structures of s-superconductor with fractional quantum Hall edge states were suggested as possible realization of parafermions, which could bring such settings closer to fault-tolerant quantum computing. Quantum Hall ferromagnet domain walls at fractional filling factors proximity-coupled to s-type superconductor can also potentially produce parafermions, making studies of helical domain walls an important area of the field of topological quantum computing.

Acknowledgments

ACKNOWLEDGMENTS

G.S., A.K., L.P.R., T.W. and Y.B.L-G. acknowledge support by the Department of Defence Office of Naval Research Award N000141410339. Work on Majorana fermions in a smooth random potential was supported by the U.S. Department of Energy, Office of Basic Energy Sciences, Division of Materials Sciences and Engineering under Award DE-SC0010544 (GS and Y.B.L-G). T.W. was partially supported by the National Science Centre (Poland) through Grant No. DEC- 2012/06/A/ST3/00247 and by the Foundation for Polish

Science through the IRA Program co-financed by EU within SG OP.

---

[1] A. Y. Kitaev, Ann. Phys. **303**, 2 (2003).

[2] C. Nayak, S. H. Simon, A. Stern, M. Freedman, and S. DasSarma, Rev. Mod. Phys. **80**, 1083 (2008).

[3] G. Moore and N. Read, Nuclear Physics B **360**, 362 (1991).

[4] R. L. Willett, Reports on Progress in Physics **76**, 076501 (2013).

[5] N. Read and E. Rezayi, Phys. Rev. B **59**, 8084 (1999).

[6] M. Barkeshli and X.-G. Wen, Phys. Rev. Lett. **105**, 216804 (2010).

[7] M. R. Peterson and S. Das Sarma, Phys. Rev. B **81**, 165304 (2010).

[8] Z. Papić, M. O. Goerbig, N. Regnault, and M. V. Milovanović, Phys. Rev. B **82**, 075302 (2010).

[9] G. Simion and Y. Lyanda-Geller, Phys. Rev. B **95**, 161111 (R) (2017).

[10] G. E. Volovik, "Fermions in the vortex core in chiral superconductors," (1997), 9709159v3 [cond.mat].

[11] L. Fu and C. L. Kane, Phys. Rev. Lett. **100**, 096407 (2008).

[12] E. Bocquillon, R. Deacon, J. Wiedenmann, P. Leubner, , T. Klapwijk, C. Bruene, K. Ishibashi, H. Buhmann, and L. Molenkamp, Nature Nanotechnology **12**, 137 (2017).

[13] R. M. Lutchyn, J. D. Sau, and S. Das Sarma, Phys. Rev. Lett. **105**, 077001 (2010).

[14] Y. Oreg, G. Refael, and F. von Oppen, Phys. Rev. Lett. **105**, 177002 (2010).

[15] V. Mourik, K. Zuo, S. M. Frolov, S. R. Plissard, E. P. A. M. Bakkers, and L. P. Kouwenhoven, Science **336**, 1003 (2012).

[16] L. P. Rokhinson, X. Liu, and J. K. Furdyna, Nat. Phys. **8**, 795 (2012).

[17] A. C. Potter and P. A. Lee, Phys. Rev. B **83**, 184520 (2011).

[18] O. Motrunich, K. Damle, and D. A. Huse, Phys. Rev. B **63**, 224204 (2001).

[19] T. Stanescu, R. M. Lutchyn, and S. D. Sarma, Phys. Rev. B **84**, 144522 (2011).

[20] R. M. Lutchyn, T. D. Stanescu, and S. Das Sarma, Phys. Rev. B **85**, 140513 (R) (2012).

[21] P. W. Brouwer, M. Duckheim, A. Romito, and F. von Oppen, Phys. Rev. B **84**, 144526 (2011).

[22] P. W. Brouwer, M. Duckheim, A. Romito, and F. von Oppen, Phys. Rev. Lett. **107**, 196804

(2011).

[23] J. D. Sau, S. Tewari, and S. Das Sarma, Phys. Rev. B **85**, 064512 (2012).

[24] J. D. Sau and S. DasSarma, Nature Communications **3**, 964 (2012).

[25] I. C. Fulga, A. Haim, A. R. Akhmerov, and Y. Oreg, New Journal of Physics **15**, 045020 (2013).

[26] T. P. Choy, J. M. Edge, A. R. Akhmerov, and C. W. J. Beenakker, Phys. Rev. B **84** (2011).

[27] I. Martin and A. F. Morpurgo, Phys. Rev. B **85**, 144505 (2012).

[28] W. DeGottardi, D. Sen, and S. Vishveshwara, Phys.Rev.Lett **110**, 146404 (2013).

[29] J. Klinovaja, P. Stano, A. Yazdani, and D. Loss, Phys. Rev. Lett **111**, 186805 (2013).

[30] M. M. Vazifeh and M. Franz, Phys.Rev.Lett **111**, 206802 (2013).

[31] S. Nadj-Perge, I. K. Drozdov, J. Li, H. Chen, S. Jeon, J. Seo, A. MacDonald, B. A. Bernevig, and A. Yazdani, Science **346**, 602 (2014).

[32] P. Zhang and F. Nori, New Journal of Physics **18**, 043033 (2016).

[33] I. Adagideli, M. Wimmer, and A. Teker, Phys. Rev. B **89**, 144506 (2014).

[34] N. H. Lindner, E. Berg, G. Refael, and A. Stern, Physical Review X **2**, 041002 (2012).

[35] D. J. Clarke, J. Alicea, and K. Shtengel, Nat. Commun. **4**, 1348 (2012).

[36] R. S. K. Mong, D. J. Clarke, J. Alicea, N. H. Lindner, P. Fendley, C. Nayak, Y. Oreg, A. Stern, E. Berg, K. Shtengel, and M. P. A. Fisher, Phys. Rev. X **4**, 011036 (2014).

[37] A. Kazakov, G. Simion, Y. Lyanda-Geller, V. Kolkovsky, Z. Adamus, G. Karczewski, T. Wojtowicz, and L. P. Rokhinson, Phys. Rev. B **94**, 075309 (2016).

[38] V. I. Fal'ko and S. Iordanskii, Phys. Rev. Lett. **84**, 127 (2000).

[39] A. Kazakov, G. Simion, Y. Lyanda-Geller, V. Kolkovsky, Z. Adamus, G. Karczewski, T. Wojtowicz, and L. P. Rokhinson, Phys. Rev. Lett. **119**, 046803 (2017).

[40] J. P. Eisenstein, H. L. Stormer, L. N. Pfeiffer, and K. W. West, Phys. Rev. B **41**, 7910 (1990).

[41] A. Y. Kitaev, Physics-Uspekhi **44**, 126 (2001).

[42] T. M. Lu, L. A. Tracy, D. Laroche, S.-H. Huang, Y. Chuang, Y.-H. Su, J.-Y. Li, and C. W. Liu, Scientific Reports **7**, 2468 (2017).

[43] S. Koch, R. J. Haug, K. v. Klitzing, and M. Razeghi, Phys. Rev. B **47**, 4048 (1993).

[44] E. De Poortere, E. Tutuc, S. Papadakis, and M. Shayegan, Science **290**, 1546 (2000).

[45] J. C. Chokomakoua, N. Goel, S. J. Chung, M. B. Santos, J. L. Hicks, M. B. Johnson, and S. Q. Murphy, Phys. Rev. B **69**, 235315 (2004).

[46] J. Jaroszyński, T. Andrearczyk, G. Karczewski, J. Wróbel, T. Wojtowicz, E. Papis, E. Kamińska, A. Piotrowska, D. Popović, and T. Dietl, Phys. Rev. Lett. **89**, 266802 (2002).

[47] C. Betthausen, P. Giudici, A. Iankilevitch, C. Preis, V. Kolkovsky, M. Wiater, G. Karczewski, B. A. Piot, J. Kunc, M. Potemski, T. Wojtowicz, and D. Weiss, Phys. Rev. B **90**, 115302 (2014).

[48] K. Lai, W. Pan, D. Tsui, S. Lyon, M. Muhlberger, and F. Schaffler, Phys. E Low-dimensional Syst. Nanostructures **34**, 176 (2006).

[49] B. E. Feldman, A. J. Levin, B. Krauss, D. A. Abanin, B. I. Halperin, J. H. Smet, and A. Yacoby, Phys. Rev. Lett. **111**, 076802 (2013).

[50] S. Kraus, O. Stern, J. G. S. Lok, W. Dietsche, K. von Klitzing, M. Bichler, D. Schuh, and W. Wegscheider, Physical Review Letters **89**, 266801 (2002).

[51] T. Wu, A. Kazakov, G. Simion, Z. Wan, J. Liang, K. West, K. Baldwin, L. N. Pfeiffer, Y. Lyanda-Geller, and L. P. Rokhinson, arXiv:1709.07928.

[52] T. Wojtowicz, M. Kutrowski, G. Karczewski, J. Kossut, F. J. Teran, and M. Potemski, Phys. Rev. B **59**, R10437 (1999).

[53] See Supplemental Material [URL will be inserted by the publisher], citing reference [58], for additional details.

[54] J. Alicea, Reports on Progress in Physics **75**, 076501 (2012).

[55] Y. Avishai, M. Y. Azbel, and S. A. Gredeskul, Physical Review B **48**, 17280 (1993).

[56] S. A. Gredeskul and M. Y. Azbel, Physical Review B **49**, 2323 (1994).

[57] E. I. Rashba, Sov. Phys. Solid State **2**, 1109 (1960).

[58] J. Furdyna, Journal of Applied Physics **64**, R29 (1988).